Exceptional integrated vapour transport toward orography: an important precursor to severe floods in Switzerland

Paul Froidevaux[1]*, Olivia Martius[1,2]

[1]*Oeschger Centre for Climate Change Research and Institute of Geography, University of Bern, Bern, Switzerland*

[2]*Mobiliar Lab for Natural Risks, University of Bern, Bern, Switzerland*

*Correspondence to: Institute of Geography, University of Bern, Hallerstrasse 12, Bern, Switzerland

E-mail: paul.froidevaux@giub.unibe.ch

Floods in mountainous regions like the Swiss Alps are still challenging to forecast because they result from very diverse hydrometeorological processes. A better understanding of large-scale flood precursors is therefore important. In this study the synoptic situations leading to 14 high-impact floods in Switzerland between 1987 and 2011 are analysed using the Era-Interim dataset.

In a first step, the flood-related synoptic flow situations are classified into four categories: i) Atmospheric rivers (ARs) with NW flow associated with floods in NW Switzerland; ii) ARs with W-SW flow associated with floods in N Switzerland; iii) pivoting potential vorticity (PV) cut-offs associated with floods in NE Switzerland and iv) PV streamers associated with floods in S Switzerland. The strong link between ARs and floods in N Switzerland is demonstrated for the first time. The four synoptic categories are associated with very different flow patterns over Switzerland but all categories correspond to intense integrated vapour transport (IVT) directed perpendicular to orography.

In a second step, the episodes of intense IVT related to the 14 floods are compared to the local climatology in terms of IVT amplitude, direction and duration. Ten of the 14 flood events correspond to exceptionally intense IVT perpendicular to orography. Despite the enormous complexity of the involved hydrometeorlogical processes, applying 4 simple thresholds of IVT toward orography at particular grid points of Era-Interim allows one to distinguish 10 flood events from all non-flood situations with only 6 non-events captured and 4 missed flood events. The close relationship between large-scale IVT and highly destructive local flood events shown here motivates the use of IVT information for medium-range flood warning systems.

Key Words: atmospheric river; atmospheric integrated vapour transport; moisture transport; heavy precipitation; flood warning

1. Introduction

The Alpine region is particularly vulnerable to floods. Precipitation typically increases with elevation in the Swiss Alps, and at higher elevations the soils are often shallower, the vegetation more open and the terrain steeper. All of these factors contribute to a rapid conversion of precipitation into surface runoff (see e.g. Weingartner *et al.* 2003). Together, floods, debris flows and landslides caused approximately 8 billion Euros of losses in Switzerland between 1972 and 2007 (Hilker *et al.* 2009). The major floods of the last 120 years occurred during typical synoptic situations such as potential vorticity (PV) cut-offs, PV streamers or zonal flow (Stucki *et al.* 2012). Although the synoptic evolution of these situations is rather well understood, it remains an open question as to what distinguishes the flood-triggering flow situations from similar situations that do not lead to floods. Understanding this difference would contribute significantly to improved flood warnings.

The major floods in Switzerland followed widespread heavy precipitation. The search for an atmospheric flood precursor may thus be conducted at the meso- to large-scale and focussed on the two main ingredients of heavy precipitation (see e.g. Doswell III *et al.* 1998): (i) a strong and sustained moisture supply and (ii) ascent of the moist air.

Moisture supply for flood events has been studied using Lagrangian analysis techniques (e.g. Martius *et al.* 2013; Grams *et al.* 2014; Winschall *et al.* 2014; Piaget *et al.* 2014). These studies have shown that moisture associated with heavy precipitation can stem from in situ inland evaporation or can be transported to the flood area from distant oceanic evaporation. The supply of moisture can also result from the combination of transport from multiple sources. Weather systems ensure the transport of moisture toward the flood area. Of particular relevance are atmospheric rivers (AR). ARs are long and narrow corridors of intense vertically-integrated water vapour transport (IVT, see e.g. Newell *et al.* 1992). They form along the fronts of extratropical cyclones; maximum moisture transport occurs in the warm sectors of the cyclones and in the pre-frontal low-level jets (see e.g. Cordeira *et al.* 2013; Dacre *et al.* 2015). ARs can extend over several thousand kilometres across oceans in the mid-latitudes and are frequently linked to tropical moisture exports (Knippertz *et al.* 2013). ARs are an important moisture source for floods along the US West Coast (see e.g. Ralph *et al.* 2006; Neiman *et al.* 2011). They are also systematically associated with the strongest winter floods in Britain (Lavers *et al.* 2011) and with a large fraction of heavy precipitation in Europe (Lavers and Villarini 2013). The transport of large quantities of moisture inland within ARs is the main reason for the association of ARs and floods.

Once a sufficient quantity of moisture is supplied, the second step in the generation of precipitation is the ascent of the moist air. A number of processes can be relevant for the lifting. Lifting of the moisture by convective systems played a crucial role in several catastrophic floods like the Big Thompson flood along the foothills of the Rocky Mountains in 1976 (Caracena *et al.* 1979) or more recent floods in southern France (Ducrocq *et al.* 2008). Dynamically forced ascent also often acts as a key ingredient to heavy precipitation and floods (Massacand *et al.* 1998; Schlemmer *et al.* 2010; Pfahl 2014; Grams *et al.* 2014). Dynamically forced ascent includes forced quasi-geostrophic lifting as well as convergence of moist air masses (Doswell III *et al.* 1998; Giannakaki and Martius 2015). Beside convective and dynamical lifting, forced orographic ascent can suffice to generate heavy precipitation in the case of intense IVT toward mountains. Orographic ascent is, for example, the main precipitation mechanism when ARs encounter the coastal mountain ridges of the US West Coast (Neiman *et al.* 2011; Dettinger 2011). The forced orographic ascent of moisture transported within ARs also recurrently results in heavy precipitation and floods over the Western US (see e.g. Ralph *et al.* 2006; Neiman *et al.* 2011; Rutz *et al.* 2014).

Similar direct large-scale flood precursors have not yet been identified for Switzerland. The challenge is linked with the complexity and diversity of flood-triggering situations in Switzerland. In N Switzerland, upper-level cyclonic systems (i.e. PV cut-offs) pivoting around the Alps are related to flood events in summer (Stucki *et al.* 2012), but a large fraction of the heavy precipitation events throughout the year is related to zonal westerly flow (see e.g. Stucki *et al.* 2012; Giannakaki and Martius

2015). In S Switzerland, heavy precipitation is strongly linked to upper-level troughs (PV streamers) located west of the Alps (see e.g. Massacand *et al.* 1998; Martius *et al.* 2006). In addition to the various large-scale situations, multiple small-scale processes tied to the complex topography can be important for flood generation. These include convection (Helbling *et al.* 2006; Diezig and Weingartner 2007; Stucki *et al.* 2012) and local interactions of the flow with topography. For example, an AR transported large amounts of moisture toward the northern Swiss Alps in October 2011 (Piaget *et al.* 2014). The precipitation that resulted from the extreme, large-scale moisture transport was only locally extreme and was related to a kilometre-scale precipitation enhancement along a small crest. Adding to the complexity, the local flooding (see Rössler *et al.* 2014) ultimately resulted from the interaction of rain and fresh snow. The snow cover is an important hydrological player in the formation of extreme discharge in Switzerland in general (Helbling *et al.* 2006; Diezig and Weingartner 2007; Stucki *et al.* 2012).

The variety of hydrometeorological mechanisms that lead to flooding at multiple scales in Switzerland makes flood forecasting very challenging. However, a close connection between large-scale IVT and heavy precipitation or floods has recently been demonstrated for areas in North America and Europe. This relationship is especially strong in mountainous regions where the condensation of moisture is primarily linked with orographic ascent (see also Lavers *et al.* 2014).

In this paper, we investigate whether the flood events in Switzerland, as diverse as they are, are nevertheless systematically related to a distinct and recurrent signal of IVT. We analyse 14 extreme floods in Switzerland during the ERA-Interim reanalysis period (1979-present, see Dee *et al.* 2011). The following section briefly presents the flood events and the data used. Section 3 then describes the flood-associated synoptic configurations, and section 4 compares the flood-associated IVT to the local climatology. Section 5 discusses one particular event in greater detail and vertical profiles are shown in section 6. Discussion, summary and conclusions follow in sections 7 and 8.

2. Data and methods

2.1. *Data*

For this study, we use Era-Interim, the latest global atmospheric reanalysis data set of the European Centre for Medium-Range Weather Forecasts (ECMWF) (see Dee *et al.* 2011). The data has 60 vertical levels between the ground and 0.1 hPa, with a higher density of levels near the surface. The spectral resolution of the model is T255 and the data are interpolated on a 1 by 1 degree latitude-longitude grid. Era-Interim covers the whole globe at a 6-hourly resolution (0, 6, 12 and 18 UTC) for the period from 1979 to present. We used information about temperature, pressure, specific humidity and the 3-dimensional wind. IVT is calculated following e.g. Lavers *et al.* (2012):

$$\mathrm{IVT} = \frac{1}{g}\sqrt{\left(\int_{p=1000}^{p=0} qu\,\mathrm{d}p\right)^2 + \left(\int_{p=1000}^{p=0} qv\,\mathrm{d}p\right)^2} \quad \left[\mathrm{kg\,m^{-1}s^{-1}}\right] \tag{1}$$

where g is the acceleration due to gravity, q is the specific humidity, u and v are the zonal and meridional wind components and p is the pressure.

We show hourly temperature and precipitation measurements taken at the automated weather station of La Chaux-de-Fonds by the Federal Office of Meteorology and Climatology MeteoSwiss. The discharge measurements are taken at the Suze River in Sonceboz by the Federal Office for the Environment FOEN. See locations in Figure 1. The selection of flood events is based on the network of river discharge stations operated by the FOEN in Switzerland (see Schmocker-Fackel and Naef 2010; Froidevaux 2014; Froidevaux *et al.* 2015).

2.2. *Selection of flood events*

For the subsequent analyses we selected the most extreme regional-scale flood events that happened in Switzerland between 1979 and 2011. Schmocker-Fackel and Naef (2010) defined regional-scale flood events in Switzerland for the period 1850-2007 from a set of 83 long term discharge stations of the FOEN network spread homogeneously over the Swiss territory. Schmocker-Fackel and Naef (2010) defined flood events as follows: more than 10% of the stations operating at the time of the flood had to register a discharge with a return period exceeding

10 years within 4 days of the event. We use the regional-scale flood events that Schmocker-Fackel and Naef (2010) identified since 1979 (11 events). In addition to Schmocker-Fackel and Naef (2010), Froidevaux (2014) recently investigated Swiss flood events using a larger sample of approximately 180 Swiss stations including more recent and shorter time series of the FOEN network. Three of the most well-known flood events since 1979 appear more important in the sample of Froidevaux (2014) than at least one of the events identified by Schmocker-Fackel and Naef (2010); i.e. a higher number of stations recorded a 5-year and/or a 10-year peak discharge. These three events which happened in October 2011 (see Rössler *et al.* 2014; Piaget *et al.* 2014), August 2000 and December 1991 are included for completeness. The final sample of 14 events encompasses the large majority of flood damages recorded in Switzerland since 1979 (Hilker *et al.* 2009). Table 1 summarizes, for each flood event, the most affected region as well as the number of river discharge time series exceeding their 5-year and 10-year empirical return periods in the station sample of Froidevaux (2014).

The exact timing of the heavy precipitation related to a flood event can vary locally. Nevertheless, considering the whole affected areas, the maximum of precipitation intensity is found on the flood date or on the day before for all events. Therefore, we investigate here the flood-related IVT within this two-day period.

3. Synoptic description of the flood events

We first subjectively classified the 14 events based on the synoptic-scale upper-level flow and the moisture transport. Following previous studies (see Massacand *et al.* 1998; Kljun *et al.* 2001; Stucki *et al.* 2012), we defined four synoptic categories: (i) ARs with NW flow, (ii) ARs with W-SW flow, (iii) pivoting cut-offs (PCOs), and (iv) PV streamers. The categories are described in the following subsections and summarized in Table 2.

3.1. ARs with NW flow

The flood events of February 1990, December 1991 and October 2011 were associated with Atlantic ARs and NW flow over Switzerland and mainly affected NW Switzerland (Table 2). These three events were preceded by a similar synoptic evolution: namely, the passage of a PV trough over the Alps followed by the establishment a pronounced PV ridge. The upper-level flow evolution was accompanied in all three cases by a sharp air mass transition at the surface. Two main phases of synoptic development can be distinguished (see also Rössler *et al.* 2014; Piaget *et al.* 2014, for October 2011):

During the first phase, the eastern edges of upper-level PV troughs (Figure 2(a,c,e)) were co-located with low level cold fronts, the passage of which led to a temperature decrease on the north side of the Alps (Figure 3(a,c,e)) and to the onset of sustained snowfall at relatively low elevations. The PV troughs then moved downstream and evolved into a PV streamer in 1991 and into a PV cut-off in 2011.

During the second phase, PV ridges following the troughs extended over large parts of the North Atlantic to the Alps (Figure 2(b,d,f)). The eastern edges of the low-level anticyclones were co-located with warm fronts (Figure 3(b,d,f)) and their arrival in northern Switzerland resulted in a rapid warming and intense rainfall on the fresh snow. Snow melt significantly contributed to the discharge peaks in all three events.

Despite a similar synoptic-scale flow evolution prior to and during the three flood events, different areas were affected. This was primarily due to different altitudes of the snow line. The 2011 flood event affected the Prealps and the northern Alps because rain on snow during phase (ii) occurred at an elevation between approximately 1500 and 3000 m.a.s.l.. In contrast, the winter floods in 1990 and 1991 mainly affected the lower-lying Jura Mountains and the Swiss Plateau because rain on snow during phase (ii) occurred between approximately 500-1500 m.a.s.l.. The hourly evolution of local temperature and precipitation for 2011 is shown in Rössler *et al.* (2014) and Piaget *et al.* (2014). At 2700 m.a.s.l. in the northern Alps, up to 80 cm of snow accumulated within one day during phase (i). Extreme rainfall started 18 hours later during phase (ii), producing 160 mm of rain in 12 hours and reducing the snow cover by 60 cm. This can be compared to the local weather evolution at 1000 m.a.s.l. in the Jura Mountains in 1990 and 1991, shown in Figure 4. For the event of 1991 (Figure 4(a)), the passage of the cold front was related to sustained snowfall; at the end of phase (i), the total snow depth amounted to 30 cm. The subsequent warm front was associated with a rapid increase in precipitation intensity and

with a change from solid to liquid precipitation at 1000 m.a.s.l.. Rainfall lasted for more than a day during phase (ii) and the fresh snow cover melted almost completely. The event evolution in 1990 was remarkably similar (see Figure 4(b)). The two events resulted in the highest discharge peaks recorded at the Suze River since measurement begin in 1961.

The most intense precipitation coincided, in each of the three cases, with the arrival of an Atlantic AR over Switzerland. Figure 5 shows, for each event, the evolution of the AR over the north Atlantic for a 5-day period finishing on the flood date. The ARs all extended far across the north Atlantic when they reached the Alps (Figure 5(m,n,o)). The three ARs developed after the convergence of two areas of intense IVT over the north Atlantic on 7 October 2011, 20 December 1991 and 12 February 1990 (Figure 5(d,h,f)). The ARs then strengthened with time across the north Atlantic (possibly due to moisture flux convergence, see Cordeira *et al.* 2013) and formed bands of intense IVT exceeding 1000 $\mathrm{kg\,m^{-1}s^{-1}}$ in the subsequent days (Figure 5(j,k,l)).

The ARs maintained intense IVT over land until they reached the Swiss orography. Lavers and Villarini (2013) showed that ARs can transport large amounts of moisture as far inland as Germany and Poland and that the northwestern Alps are a hot spot for AR contribution to heavy precipitation. Rutz *et al.* (2014) showed that the ability of ARs to maintain intense IVT over land is closely related to their inland trajectory and to whether they can avoid vapour depletion by major orographic obstacles along the way.

The three ARs were located along the northern edges of anticyclones positioned near Iberia (Figure 2). The locations of the anticyclones and the corresponding northward excursions of the ARs before they reached Switzerland had several consequences for the heavy precipitation over Switzerland. Firstly, the ARs made landfall over northern France or the British Isles so that they crossed no major orographic obstacle before impinging on the Jura and the Alps. In contrast, many ARs make landfall SW of the Alps and reach Switzerland after having already been depleted by their previous passage over the Sierra Nevada, the Pyrenees and/or the Massif Central (see e.g. Fazan 2014). Secondly, the ARs crossed land downstream of the anticyclones, i.e. in environments typically dominated by negative vorticity advection. This may have contributed to hinder water depletion by precipitation. Thirdly, the ARs reached Switzerland from a NW direction so that the IVT was almost perpendicular to the WSW-ENE oriented main chains of the Jura Mountains and the Alps. The ARs thus impinged on the orography and were rapidly depleted over NW Switzerland.

In summary, the case studies show three intense Atlantic ARs reaching NW Switzerland from a northwesterly direction, thereby transporting large quantities of moisture toward the orography. Section 4 addresses quantitatively how unusual the amplitude, direction and duration of the IVT whithin these ARs was by comparing it to the IVT climatology over NW Switzerland.

3.2. *ARs with W-SW flow*

The flood events on May 1999 in NE Switzerland and on 26 September 1987 in NW Switzerland were related to ARs with IVT from the sector W-SW over N Switzerland (see Table 2). During the event of May 1999, an anticyclone was located over southwestern Europe and northwestern Africa and the mid-tropospheric flow was zonal over Switzerland (see Figure 6(a)). An Atlantic AR located along the northern edge of the anticyclone reached N Switzerland from the west (Figure 6(c), see also Stucki *et al.* 2012). In contrast to the three ARs with NW flow described previously, this AR corresponds to WSW IVT over N Switzerland, i.e. a transport of moisture parallel to the main Alpine chain.

In September 1987, another AR was related to intense WSW IVT over NW Switzerland and toward the Jura Mountains, where the heaviest precipitation and the most extreme discharges were recorded. Figure 6(d) shows a band of intense IVT extending from the Mediterranean to NW Switzerland and reaching it from the SW through the Rhone Valley. The associated chart of geopotential height at 500 hPa and temperature at 850 hPa is shown in Figure 6(b).

The IVT during these two events was as intense as for the three ARs with NW flow described previously but it was not oriented toward the main topographic barrier.

3.3. *PCOs*

Five flood events were associated with upper-level PV cut-offs pivoting around the Alps from the west, to the south and to

the east (abbreviated here as PCOs for pivoting cut-offs). These events mainly affected NE Switzerland (see Table 2). PCO patterns correspond to the early phase of the Vb cyclone track (Van Bebber 1891), which is well known for causing damaging floods in Central and Eastern Europe (see e.g. Ulbrich *et al.* 2003; Kundzewicz *et al.* 2005). Upper-level PCOs typically co-occur with surface cyclones that pass south of the Alps and over the Mediterranean before recurving northwards. These cyclones can bring warm, moist and weakly stratified air toward Central Europe. Depending on the exact cyclone track after recurving around the Alps, the warm and moist air may rain out over Central Europe or reach the north side of the Alps and lead to orographically-enhanced precipitation. PCO-related floods in Switzerland are well-studied and we refer to the literature for the details (see e.g. Kljun *et al.* 2001; Hohenegger *et al.* 2008; FOEN 2008; Stucki *et al.* 2012).

Figure 7 shows IVT and PV charts during the episodes of intense IVT related to the five flood events. Closed contours of the 2 pvu isoline show the location of a cut-off south-southeast of Switzerland (except for 2007 when the cut-off was still located in the west). The cut-offs are associated with cyclonic circulations extending down to the low levels. The cyclonic circulations are visible as counter clockwise patterns of intense IVT encircling the Alps and impinging on the Alps over NE Switzerland from directions between NNW and ENE. The IVT values north of the Alps hardly exceed $300\,\mathrm{kg\,m^{-1}\,s^{-1}}$ and are relatively low compared to the IVT values during the events related to ARs with NW flow and ARs with W-SW flow.

Like the ARs described above, the five PCOs correspond to a systematic and distinct IVT pattern. In section 4, we compare the investigated IVT episodes to the IVT climatology of NE Switzerland and consider intensity, direction and duration. We address whether IVT values of approximately $300\,\mathrm{kg\,m^{-1}\,s^{-1}}$ from NNW-ENE have systematically severe consequences or whether such IVT values also regularly occur without generating exceptional flood events.

3.4. PV streamers

The four regional-scale floods that have affected southern Switzerland since 1987 were all associated with a positive PV anomaly located west of the Alps. Positive PV anomalies located west of the Alps (typically PV streamers, some of them evolving into PV cut-offs) are well-known for generating heavy precipitation on the Alpine south-side (Massacand *et al.* 1998; Rotunno and Ferretti 2001; Martius *et al.* 2006; Hoinka and Davies 2007; Schlemmer *et al.* 2010). The exact location and shape of the positive PV anomaly vary between the four events but all anomalies correspond to intense IVT along their eastern edge and toward the Swiss Alpine south-side. The direction of IVT is closely related to the affected regions: SW Switzerland was affected by SSE IVT toward the Alps in October 2000 and September 1993 (Figure 8(a,b), see also Hoinka and Davies (2007) for 1993), S Switzerland was affected by S IVT in August 1987 (Figure 8(c)) and SE Switzerland was affected by SSW IVT in July 1987 (Figure 8(d)).

4. Climatological analysis of IVT

4.1. ARs with NW flow

ARs with NW flow mainly affected NW Switzerland. The ERA-interim grid point at 47°N-7°E (marked with the letter J in Figure 1) is selected to represent this region. The IVT climatology at 47°N-7°E, i.e. the IVT values for each 6-hourly time step between 1979 and 2011, is shown in Figure 9. IVT is most frequent from WSW for all intensities; a second maximum is found from ENE. These two preferential directions reflect the frequent occurrence of along-topography jets (the orientation of the Jura and the western Swiss Alps is approximately WSW-ENE), with a clear domination of the westerly flow. Although extreme IVT from NW to SW can be found in all seasons, extreme IVT from NE occurs almost exclusively in summer and extreme IVT from SE occurs almost exclusively in spring and fall.

The highest IVT values corresponding to the flood events related to ARs with NW flow are marked and connected by solid lines in Figure 9. For example, the connected squares correspond to the event on 10 October 2011 (09 October 2011 18 UTC, 10

October 2011 00 UTC and 10 October 2011 06 UTC). The flood-related IVT values are the most intense in 33 years from their respective directions (from NNW in the 2011 case, from NW in 1991 and from WNW in 1990). If we assume the Swiss topography is aligned in an approximately WSW-ENE direction, we can calculate the IVT perpendicular to the orography. A threshold of 350 kg m^{-1} s^{-1} perpendicular to the orography was only exceeded 14 times in 33 years. Of the 14 occurrences, 11 happened during the three flood events (see also Table 3).

The IVT diagram shows that the three events are in line with the simplest concept of orographic precipitation: The worst flood events were recorded when the highest amount of moisture was transported toward the orography, forced to rise, condense, and generate extreme precipitation. Complex local hydrometeorological processes related to the complex terrain and the snow melt strongly contributed to the river discharges during these events. These processes had a pronounced local character but they occurred during exceptional large-scale IVT conditions.

The other exceedances of the IVT threshold in 33 years happened in relation to similar ARs with NW flow on 05 December 1988 (one exceedance) and 01 August 1997 (two exceedances). These two ARs, although not related to extreme river discharge, were associated with heavy precipitation (up to 100 mm in 24 h over NW Switzerland in 1988 and up to 50 mm in 48 h over N Switzerland in 1997).

The IVT diagram focuses on the 6-hourly IVT. We investigate the duration of the extreme IVT episodes by calculating intensity-duration-frequency (IDF) curves of IVT. IDF information of the IVT climatology at 47°N-7°E is shown in Figure 10 for three directional sectors. To obtain the IDF climatology, zonal and meridional IVT are first averaged for durations between 6 hours to 7 days over the 33 years. The mass flux-weighted mean direction is calculated and all values with a mean direction from a particular sector are considered in the sector-wise IDF climatology. To construct the IDF curves of the flood events, the maximum averaged IVT values for each duration are extracted from the 7-day period preceding the flood dates (flood dates included). For the sector NW-N (315°-360°) in Figure 10(a), the events of 2011 and 1991 coincide with the most intense IVT episodes maintained over durations ranging from 6 hours to one day. The IVT intensity during the event of 1991 was also the most intense for durations between 4 and 7 days. For the sector W-NW in Figure 10(b), the event of 1990 sets records for durations between 12 hours and 3 days.

The duration offers a complementary information to appreciate the extremeness of the flood-related IVT episodes. The three flood events related to ARs with NW flow correspond to the highest IVT intensities, but also to the most persistently intense IVT from their particular sector for durations of up to several days. The heavy precipitation periods of these events lasted for approximately one day, but they were preceded by precipitation (mostly snowfall) from the same sector and starting around 3-4 days prior to the floods.

4.2. *ARs with W-SW flow*

The two flood events related to ARs with W-SW flow occurred on 12 May 1999 and on 26 September 1987. The IVT related to these events is shown by dashed lines in Figure 9. Both events include at least one time step among the 1% most intense IVT from W-SW. However, these IVT episodes were neither exceptional nor oriented toward the main Alpine chain. More intense IVT from W-SW occurred repeatedly without resulting in exceptional flooding. The consideration of the IVT IDF curves for both events in Figure 10(c) reveals that the IVT episodes did not exceed the percentile 99.9 of the IVT climatology from SW-W for any duration between 6 hours and 7 days. Of course, these two flood events -like the other events- resulted from a complex interaction of several meteorological and hydrological factors (e.g., snow melt was particularly important for the event of May 1999). Thus, multiple precipitation- and discharge-enhancing factors may explain why very intense but non-extreme IVT ultimately resulted in extreme floods.

4.3. *PCOs*

The flood events related to PCOs correspond to IVT from approximately NE over Switzerland and mainly affected NE Switzerland. The IVT climatology is thus analysed at the grid point 48°N-9°E, which lies just upstream of NE Switzerland in the case of NE flow (see Figure 11).

All flood events were linked to exceptionally intense IVT, with

the exception of the flood event of August 2007, during which the IVT remained weak. An IVT component of 300 kg m^{-1} s^{-1} from sector NNW-NE is best suited to separate the flood events from all other time steps. This threshold was exceeded only 18 times in 33 years (see Table 3). Of the 18 exceedances, 11 correspond to the events of 1999, 2000, 2002 and 2005.

Considering the IVT IDF in Figure 12, the IVT during the event of 2005 was the most intense in 33 years for durations of 6-54 hours. In contrast, the events of 2002, 2000 and 1999 only correspond to exceptional isolated IVT time steps, while the maximum IVT at longer durations is not climatologically outstanding.

Like the ARs with NW flow, 4 of the 5 PCO events correspond to the most extreme IVT episodes ever experienced when intensity, direction and duration are considered. Very long durations are not required for flood generation and the maintenance of exceptionally intense IVT for 18 h sufficed to generate exceptional floods in May 1999, for example. Nevertheless, the combination of exceptional intensity and persistence in August 2005 led to the most catastrophic flood of the last century. The flood event of August 2007, which lacked very intense IVT, is discussed later.

The 7 other exceedances of the IVT threshold happened during similar PCO situations on 17 June 1979, 23 June 2009 and 03 June 2010 that were associated with heavy precipitation of up to approximately 80 mm, 30 mm and 50 mm in 24 hours over NE Switzerland, respectively.

4.4. PV streamers

The flood events related to PV streamers correspond to IVT from approximately S and mainly affected S Switzerland. The IVT climatology is thus analysed at the grid point 46°N-9°E, which is located just upstream of S Switzerland in the case of S flow (see Figure 13). The IVT during the events of October 2000 and September 1993 in SW Switzerland correspond to the only exceedances of 400 kg m^{-1} s^{-1} from SSE. The event of August 1987 in S Switzerland corresponds to one of the two exceedances of 550 kg m^{-1} s^{-1} from S (see Table 3). In contrast, the event of July 1987 in SE Switzerland is associated with high, but not exceptional values of IVT from SSW.

The only other exceedance of 550 kg m^{-1} s^{-1} from S occurred on 20 September 1999. This exceedance happened during an intense IVT episode that produced up to 350 mm of precipitation in 48 hours over S Switzerland and 19 annual discharge peaks.

The IDF curves of IVT in Figure 14 further highlight the exceptional character of the flood events, as the flood-related IVT episodes set records for durations ranging from 6 hours to 6 days. The event of July 1987 is the only event investigated in this study that does not contain any exceptional 6-hourly time step but involves record IVT values at longer durations.

5. An extreme flood event lacking very intense IVT

The August 2007 flood event in NE Switzerland stands out as the only event not related to very intense IVT. The NE IVT never exceeded the 90th percentile for any duration between 6 hours and 7 days (Figure 12). The synoptic situation triggering the event of 2007, a PCO, was typical for summer floods. However, during the time of heavy precipitation over N Switzerland, the PCO was located more to the west as compared to all other PCO-related cases (Figure 7(a)).

Vertical profiles from balloon soundings in Payerne and Era-Interim during the period of the heaviest precipitation (between 08 August 12 UTC and 09 August 00 UTC) reveal a counterflow situation over N Switzerland related to the presence of a cold front: a post-frontal NW flow prevailed below 700 hPa and a SE flow prevailed above (not shown). This situation resulted in relatively low IVT values partly because of the directional dependence of the IVT calculation (see Equation 1). The highest IVT value for 2007 in Figure 11 amounts to 109 kg m^{-1} s^{-1} and consists of a N partial IVT of 105 kg m^{-1} s^{-1} below 700 hPa and an ESE partial IVT of 78 kg m^{-1} s^{-1} above. If the moisture flux would have been unidirectional and of the same intensity, the IVT would have amounted to 260 kg m^{-1} s^{-1}. However, the partial IVT that is oriented toward orography (below 700 hPa) is relatively weak and the extreme precipitation must have a different cause.

Profiles of the vertical velocity over the northern Swiss Alps in Figure 15 show that ascent in 2007 peaked at 500 hPa and reached -90 hPa h^{-1}. In contrast, the ascent for all other PCO events peaked at 700 hPa and did not exceed -50 hPa h^{-1}. Figure 15 suggests that the ascent in 2007 was not orographically driven. We calculated the dynamical forcing for lifting following

Doswell III *et al.* (1998) and found widespread quasi-geostrophic vertical forcing consistent with the approaching upper-level cut-off. Era-Interim is not suited for a more precise evaluation of the flow over the Alps and we refer to a convection-resolving numerical reanalysis of the event by Piaget (2015) for more details about the local flow. The reanalysis of Piaget (2015) is consistent with an important condensation within the SE flow above 700 hPa and contribution of moisture and hydrometeors from the southern alpine side to the precipitation over northern Switzerland. Piaget (2015) also reveals the contribution of convection to the total precipitation.

The 2007 event is hence notable because precipitation happened in the lee of the orography (considering the SE flow) and was probably primarily related to dynamical lifting and convection rather than orographic lifting.

6. Vertical profiles and stability

The IVT toward orography reflects the amount of moisture that is supplied for the generation of orographic precipitation. The vertical distribution of moisture and atmospheric stability are two important environmental parameters that influence the conversion of water vapour into precipitation over orography (see e.g. Chow *et al.* 2012). A detailed investigation of the meso- to micro-scale precipitation mechanisms during the 14 events is beyond the scope of our study and requires a higher resolution than that of Era-Interim. Era-Interim nevertheless benefits from the assimilation of data from two weather balloon launching stations within the study area (at Payerne and Milano, see Figure 1). We thus investigate vertical profiles from Era-Interim during the 14 events but limit the discussion to a general description of their similarities and specificities.

The exact profiles are specific to each case and evolve throughout the events. Three exemplary profiles are shown in Figure 16 to guide the discussion. They represent the events related to ARs with NW flow (Figure 16(a)), PCOs (Figure 16(b)) and PV streamers (Figure 16(c)). Figure 16(a) shows the profile of the 2011 event as an example of the ARs with NW flow (see also Rössler *et al.* 2014). A moist neutral layer extended from 800-650 hPa and directly above a very stable layer between the ground and 800 hPa. The stable layer was blocked and the WSW low-level winds were oriented along the topography while the moist neutral layer above was oriented toward the topography. All 3 events related to ARs with NW flow show a moist neutral layer over a stable blocked layer. Figure 16(b) shows the profile of the 2005 PCO event. The air was nearly saturated and close to moist neutrality from the ground to 600 hPa and the flow was oriented toward the orography in the mid and low levels. In contrast to the situation shown in Figure 16(a), there was no low level blocking. The profiles for the PCO event of 1999 also show no blocking, and only shallow blocked layers were present in 2002 and 2000 below the nearly saturated moist neutral layers. During the PV streamer events, nearly saturated layers close to moist neutrality were also found at mid and low levels (see e.g. the 1993 event in Figure 16(c)).

In summary, the heavy precipitation periods of all 14 events correspond to nearly saturated moist neutral layers extending through several kilometres between the ground and 600 hPa. Blocked surface layers were found only for the cases related to ARs with NW flow. The 3 ARs with NW flow followed warm fronts. The low-level cold and stable layers consisted of the remains of the cold air ahead, while the moist neutral layers above consisted of the post-frontal air mass; i.e. the ARs themselves. Low-level blocking may have influenced the distribution of precipitation by pre-lifting the ARs before they impinged on the main Alpine ridge (see e.g. Figure 19 of Neiman *et al.* 2002, for a conceptual schematic). The blocked layers also affect the IVT. In 2011 for example, the NNW IVT results from the combination of a weak WSW flow below 800 hPa and a N flow above. Although the flow over the barrier is directly from N, the IVT is from NNW. Regarding thermal instability, convective available potential energy (CAPE) was around zero for all cases in northern Switzerland and less than 700 $\mathrm{J\,kg^{-1}}$ for the cases in southern Switzerland. These values are low compared to the ones during severe flood-triggering convective events in southern France, for example (about 1500-2500 $\mathrm{J\,kg^{-1}}$, see e.g. Ducrocq *et al.* 2008). A detailed evaluation of the role of convection in major Swiss floods would, however, require further analysis. Deep convection can develop with low CAPE and Era-Interim may lack the resolution to properly resolve the sounding structure at the

location were the convection is initiated. Convection-resolving numerical reanalyses from Hohenegger *et al.* (2008) and Piaget (2015) indicate that convection contributed, at least, to the events associated with PV-streamers in September 1993 and October 2000 and to the events associated with PCOs in August 2005 and August 2007.

7. Discussion

Our study is based on IVT derived from coarse resolution reanalysis data with a temporal resolution of 6 hours. Here we comment on the limitations of the approach and possible applications.

The first limitation pertains to the exact location of the flood events. The IVT diagnostic is very successful in indicating the occurrence of a flood event in relatively large areas (e.g. NW, NE, SW, S or SE Switzerland) but it does not provide information on where exactly the flood event will happen (e.g. in the Jura mountains or in the Alps). More information on the vertical profiles of temperature, moisture and stability is needed to address this question. This may be, for example, related to the presence of blocked flow in the lowest layers as observed in the events related to ARs with NW flow.

Indeed, highly variable wind profiles are a main limitation of the IVT diagnostic as they affect the IVT calculation. If there is strong directional shear between the flow in the blocked layer and the flow above, IVT direction and amplitude no longer represent the flow toward and over the orography. An extreme example of the effect of strong directional shear is the August 2007 flood event, where the total IVT was weak and consisted of northerly winds near the surface and southerly winds at higher altitudes. A refinement of the presented IVT framework would be to calculate partial IVT for several altitude ranges (see Cordeira *et al.* 2013, for example). However, the variability of the blocked layer depths make the definition of a set of standard altitude ranges and hence the case-to-case comparability difficult.

The main limitation of the IVT diagnostic is probably that it excludes all processes related to the transformation of atmospheric moisture into river discharge (e.g. related to cloud physics, snow-melt or soil moisture). Here, we relate the occurrence of highly damaging floods to a one-dimensional variable (the IVT toward orography at a single grid point of a global reanalysis). We reduce our analysis to a very simple form in order to highlight the particular importance of IVT.

Nevertheless, the strong relationship found here between IVT and the major Swiss floods indicates that, even if the highly damaging Swiss floods resulted from a complex combination of diverse processes, the large scale IVT may be the root cause of the majority of them.

An IVT-based forecasting tool for local flood events requires two conditions to work well: (i) a close relationship between IVT and local floods so that flood events can be captured by simple criteria with reasonable numbers of false alarms and missed events, and (ii) a good predictability of the IVT intensity and direction.

Our study focuses on condition (i). The results in Table 3 show that by applying a set of thresholds of IVT perpendicular to orography, 10 of the flood events can be separated from other time steps with a low number of false alarms. However, here the criteria are set after the floods occurred and are thus optimised for the sample of 14 flood events considered. A quantification of the forecasting skill would require a proper definition of calibration and validation periods. Moreover, a purely IVT-based forecasting tool would systematically miss events like the ones of August 2007, early May 1999 and September 1987, which were not related to extreme IVT. The analysis thus highlights the potential for an IVT-based flood forecasting tool as a complement to current flood forecasting systems in Switzerland, but not as a stand-alone forecasting system. Such a tool may for example be designed like the IVT-based precipitation-forecasting model presented by Neiman *et al.* (2009) and may allow to issue flood warnings for NW, NE, SW, S and SE Switzerland.

Regarding condition (ii), a recent study by Lavers *et al.* (2014) shows that the medium-range predictability of IVT is higher than that of precipitation over Western Europe; the skilful forecast horizon of IVT is up to three days longer than that of precipitation. Based on the results of Lavers *et al.* (2014), further studies are required to investigate the predictability of IVT at the particular locations considered here.

The unpredicted flood event of 2011 is a promising case since preliminary investigations show that the IVT direction and intensity were correctly predicted 1.5 days in advance by the

ECMWF high-resolution global model. In contrast, the flood-relevant local precipitation depths were underestimated by up to 50% at a 12 hours lead time by the high resolution operational model of MeteoSwiss COSMO-2 (Rössler *et al.* 2014). A simple comparison of the forecasted IVT with the local climatology at 47°N-7°E would have revealed a potentially dangerous situation. A statement in the form of: "An IVT of the direction and intensity like the one forecasted for tomorrow has occurred only twice since 1979, each time leading to a major flood" would have been possible. A simple flood forecasting system based on the IVT diagram in Figure 9 would have recognized the flood potential through comparison with the analogue cases in 1990 and 1991.

8. Summary and conclusions

The investigation of the synoptic configurations related to 14 severe floods in Switzerland between 1987 and 2011 revealed the following recurrent flood-triggering situations:

(i) Atlantic ARs with NW flow over N Switzerland were associated with major floods mainly in NW Switzerland in October 2011, December 1991 and February 1990.

(ii) ARs with W-SW flow over N Switzerland were associated with major floods in N Switzerland in early May 1999 and September 1987.

(iii) Pivoting PV cut-offs (PCOs) related to a cyclonic transport of moisture around the Alps were associated with major floods mainly in NE Switzerland in August 2007, August 2005, August 2002, August 2000 and late May 1999.

(iv) PV streamers and PV cut-offs located to the west of the Alps were associated with major floods in SW Switzerland in October 2000 and September 1993, in S Switzerland in August 1987, and in SE Switzerland in July 1987.

Ten of the 14 flood events investigated correspond to exceptionally intense IVT perpendicular to orography. Setting a threshold of IVT toward orography at the Era-Interim grid point just upstream of the affected areas is sufficient to separate the majority of the flood events from almost all other 6-hourly time steps during the 33-year time period. We define 4 thresholds of IVT from particular sectors and at particular grid points. The 4 thresholds of IVT were exceeded during 36 6-hourly time steps in 33 years. Of the 36 exceedances, 25 are related to 10 of the 14 flood events investigated and 11 correspond to 6 non-events. The 6 non-events, although not related to major floods, all correspond to widespread heavy precipitation in Switzerland.

The picture is more complex for the remaining 4 flood events. During the flood event related to a PV streamer on August 1987, the maximum 6-hourly IVT was not outstanding but the IVT was exceptional when averaged over durations of 1 to 4 days. The two events related to ARs with W-SW flow in early May 1999 and September 1987 correspond to very intense but not exceptional IVT. Finally, the PCO-related flood event of August 2007 is the only event during which the IVT intensity was never exceptionnal nor very intense.

The duration of the extreme IVT episodes is a relevant supplementary information, but it is not as determinant as the peak intensity and direction. The exceptionally intense episodes of moisture transport associated with the floods investigated here were not sustained for exceptionally long periods of time, lasting approximately 12 to 48 hours.

Floods are difficult to forecast over the complex topography of Switzerland. They often involve complex local effects and the interaction of processes like rain on snow. The results presented here suggest that local flood events may be recognised in advance thanks to their large-scale precursor IVT patterns, which may be more predictable than large-scale precipitation and are certainly more predictable than local river discharge. Future work is required on the predictability of the IVT in order to confirm its potential as an early flood precursor.

Acknowledgements

The authors gratefully acknowledge MeteoSwiss for providing access to the Era-Interim reanalysis of the ECMWF. MeteoSwiss also provided surface station measurements and radar data that were used directly and indirectly for the analysis presented here. We are also thankful to the FOEN for providing river discharge data. We would like to thank Jim Steenburgh and Nicolas Piaget for their helpful suggestions and Paraskevi Giannakaki for providing calculations of the quasi-geostrophic dynamical forcing. We also acknowledge three anonymous reviewers for their pertinent and constructive comments.

References

Caracena F, Maddox RA, Hoxit LR, Chappell CF. 1979. Mesoanalysis of the Big Thompson storm. *Mon. Weather Rev.* **107**: 1–17.

Chow F, Snyder B, Wekker S. 2012. *Mountain Weather Research and Forecasting: Recent Progress and Current Challenges*. Springer: Dordrecht, Netherlands.

Cordeira JM, Ralph FM, Moore BJ. 2013. The Development and Evolution of Two Atmospheric Rivers in Proximity to Western North Pacific Tropical Cyclones in October 2010. *Mon. Weather Rev.* **141**: 4234–4255.

Dacre HF, Clark PA, Martinez-Alvarado O, Stringer MA, Lavers DA. 2015. How do atmospheric rivers form? *Bull. Amer. Meteor. Soc.* **96**: 1243–1255.

Dee D, Uppala S, Simmons A, Berrisford P, Poli P, Kobayashi S, Andrae U, Balmaseda M, Balsamo G, Bauer P, *et al.* 2011. The ERA-Interim reanalysis: Configuration and performance of the data assimilation system. *Q. J. R. Meteorol. Soc.* **137**: 553–597.

Dettinger M. 2011. Climate Change, Atmospheric Rivers, and Floods in California–A Multimodel Analysis of Storm Frequency and Magnitude Changes. *J AM WATER RESOUR AS* **47**: 514–523.

Diezig R, Weingartner R. 2007. Hochwasserprozesstypen-: Schlüssel zur Hochwasserabschätzung. *Wasser und Abfall* **4**: 18–26.

Doswell III CA, Ramis C, Romero R, Alonso S. 1998. A diagnostic study of three heavy precipitation episodes in the western Mediterranean region. *Weather Forecasting* **13**: 102–124.

Ducrocq V, Nuissier O, Ricard D, Lebeaupin C, Thouvenin T. 2008. A numerical study of three catastrophic precipitating events over southern France. II: Mesoscale triggering and stationarity factors. *Q. J. R. Meteorol. Soc.* **134**: 131–145.

Fazan V. 2014. North Atlantic atmospheric rivers in the ERA-Interim dataset: Detection, climatology and link to Swiss floods. Master's thesis, University of Berne, Berne, Switzerland.

FOEN. 2008. The floods of 2005 in Switzerland. Synthesis report on the event analysis. Technical report.

Froidevaux P. 2014. Meteorological characterisation of floods in Switzerland. PhD thesis, University of Berne, Berne, Switzerland.

Froidevaux P, Schwanbeck J, Weingartner R, Chevalier C, Martius O. 2015. Flood triggering in Switzerland: the role of daily to monthly preceding precipitation. *Hydrol. Earth Syst. Sci.* **19**: 3903–3924.

Giannakaki P, Martius O. 2015. Synoptic-scale flow structures associated with extreme precipitation events in northern Switzerland. *Int. J. Climatol.* doi: 10.1002/joc.4508.

Grams CM, Binder H, Pfahl S, Piaget N, Wernli H. 2014. Atmospheric processes triggering the central European floods in June 2013. *Nat. Hazards Earth Syst. Sci.* **14**: 1691–1702.

Helbling A, Kan C, Vogt S. 2006. Dauerregen, Schauer oder Schmelze – welche Ereignisse lösen in der Schweiz die Jahreshochwasser aus? *Wasser Energie Luft* **98**: 249–254.

Hilker N, Badoux A, Hegg C. 2009. The Swiss flood and landslide damage database 1972-2007. *Nat. Hazards Earth Syst. Sci.* **9**: 913–925.

Hohenegger C, Walser A, Langhans W, Schär C. 2008. Cloud-resolving ensemble simulations of the August 2005 Alpine flood. *Q. J. R. Meteorol. Soc.* **134**: 889–904.

Hoinka KP, Davies HC. 2007. Upper-tropospheric flow features and the Alps: An overview. *Q. J. R. Meteorol. Soc.* **133**: 847–865.

Kljun N, Sprenger M, Schär C. 2001. Frontal modification and lee cyclogenesis in the Alps: A case study using the ALPEX reanalysis data set. *Meteorol. Atmos. Phys.* **78**: 89–105.

Knippertz P, Wernli H, Gläser G. 2013. A global climatology of tropical moisture exports. *J. Clim.* **26**: 3031–3045.

Kundzewicz Z, Ulbrich U, Brücher T, Graczyk D, Krüger A, Leckebusch G, Menzel L, Pińskwar I, Radziejewski M, Szwed M. 2005. Summer floods in Central Europe–climate change track? *Nat. Hazards* **36**: 165–189.

Lavers D, Allan R, Wood E, Villarini G, Brayshaw D, Wade A. 2011. Winter floods in Britain are connected to atmospheric rivers. *Geophys. Res. Lett.* **38**. L23803.

Lavers DA, Pappenberger F, Zsoter E. 2014. Extending medium-range predictability of extreme hydrological events in Europe. *Nat. Commun.* **5**.

Lavers DA, Villarini G. 2013. The nexus between atmospheric rivers and extreme precipitation across Europe. *Geophys. Res. Lett.* **40**: 3259–3264.

Lavers DA, Villarini G, Allan RP, Wood EF, Wade AJ. 2012. The detection of atmospheric rivers in atmospheric reanalyses and their links to British winter floods and the large-scale climatic circulation. *J. Geophys. Res.* **117**. D20106.

Martius O, Sodemann H, Joos H, Pfahl S, Winschall A, Croci-Maspoli M, Graf M, Madonna E, Mueller B, Schemm S, Sedláček J, Sprenger M, Wernli H. 2013. The role of upper-level dynamics and surface processes for the Pakistan flood of July 2010. *Q. J. R. Meteorol. Soc.* **139**: 1780–1797.

Martius O, Zenklusen E, Schwierz C, Davies H. 2006. Episodes of Alpine heavy precipitation with an overlying elongated stratospheric intrusion: A climatology. *Int. J. Climatol.* **26**: 1149–1164.

Massacand A, Wernli H, Davies H. 1998. Heavy precipitation on the alpine southside: An upper-level precursor. *Geophys. Res. Lett.* **25**: 1435–1438.

Neiman PJ, Ralph FM, White A, Kingsmill D, Persson P. 2002. The statistical relationship between upslope flow and rainfall in California's coastal mountains: Observations during CALJET. *Mon. Weather Rev.* **130**: 1468–1492.

Neiman PJ, Schick LJ, Ralph FM, Hughes M, Wick GA. 2011. Flooding in western washington: The connection to atmospheric rivers. *J. Hydrometeorol.* **12**: 1337–1358.

Neiman PJ, White AB, Ralph FM, Gottas DJ, Gutman SI. 2009. A water vapour flux tool for precipitation forecasting. *J. Water Manage.* **162**: 83–94.

Newell RE, Newell NE, Zhu Y, Scott C. 1992. Tropospheric rivers?–A pilot study. *Geophys. Res. Lett.* **19**: 2401–2404.

Pfahl S. 2014. Characterising the relationship between weather extremes in Europe and synoptic circulation features. *Nat. Hazards Earth Syst. Sci.* **14**: 1461–1475.

Piaget N. 2015. Meteorological characterizations of extreme precipitation and floods in Switzerland. PhD thesis, ETH Zurich, No 22702, Zurich, Switzerland.

Piaget N, Froidevaux P, Giannakaki P, Gierth F, Martius O, Riemer M, Wolf G, Grams CM. 2014. Dynamics of a local Alpine flooding event in October 2011: moisture source and large-scale circulation. *Q. J. R. Meteorol. Soc.* **141**: 1922–1937.

Ralph F, Neiman P, Wick G, Gutman S, Dettinger M, Cayan D, White A. 2006. Flooding on California's Russian River: Role of atmospheric rivers. *Geophys. Res. Lett.* **33**. L13801.

Rössler O, Froidevaux P, Börst U, Rickli R, Martius O, Weingartner R. 2014. Retrospective analysis of a nonforecasted rain-on-snow flood in the Alps - a matter of model limitations or unpredictable nature? *Hydrol. Earth Syst. Sci.* **18**: 2265–2285.

Rotunno R, Ferretti R. 2001. Mechanisms of intense Alpine rainfall. *J. Atmos. Sci.* **58**: 1732–1749.

Rutz JJ, Steenburgh WJ, Ralph FM. 2014. Climatological characteristics of atmospheric rivers and their inland penetration over the western United States. *Mon. Weather Rev.* **142**: 905–921.

Schlemmer L, Martius O, Sprenger M, Schwierz C, Twitchett A. 2010. Disentangling the Forcing Mechanisms of a Heavy Precipitation Event along the Alpine South Side Using Potential Vorticity Inversion. *Mon. Weather Rev.* **138**: 2336–2353.

Schmocker-Fackel P, Naef F. 2010. More frequent flooding? Changes in flood frequency in Switzerland since 1850. *J. Hydrol.* **381**: 1–8.

Stucki P, Rickli R, Brönnimann S, Martius O, Wanner H, Grebner D, Luterbacher J. 2012. Weather patterns and hydro-climatological precursors of extreme floods in Switzerland since 1868. *Meteorol. Z.* **21**: 531–550.

Ulbrich U, Brücher T, Fink A, Leckebusch G, Krüger A, Pinto J. 2003. The central European floods of August 2002: Part 2–Synoptic causes and considerations with respect to climatic change. *Weather* **58**: 434–442.

Van Bebber WJ. 1891. Die Zugstrassen der barometrischen Minima nach den Bahnenkarten der deutschen Seewarte für den Zeitraum 1875–1890. *Meteorol. Z.* **8**: 361–366.

Weingartner R, Barben M, Spreafico M. 2003. Floods in mountain areas—an overview based on examples from Switzerland. *J. Hydrol.* **282**: 10–24.

Winschall A, Sodemann H, Pfahl S, Wernli H. 2014. How important is intensified evaporation for Mediterranean precipitation extremes? *J. Geophys. Res.* **119**: 5240–5256.

Table 1. The 14 regional-scale flood events selected for this study. The flood dates in column 1 represent the days when the highest number of peak discharges were recorded in a sample of approximately 180 Swiss river discharge stations (see Froidevaux 2014, for a brief description and a map of the stations). The most affected region is shown in column 2 (see the regions in Figure 1). The number of stations that recorded a discharge peak exceeding that of the 5-year return period within -2 and +4 days of the indicated flood date is shown in column 3. Column 4 shows the same for the 10-year return period.

Date	Affected region	RP >5y	RP >10y
10 Oct 2011	NW	14	12
08 Aug 2007	NE	64	47
22 Aug 2005	NE	74	55
12 Aug 2002	NE	22	8
15 Oct 2000	SW	23	13
06 Aug 2000	NE	13	5
22 May 1999	NE	21	13
12 May 1999	NE	38	22
24 Sep 1993	SW	17	10
22 Dec 1991	NW	14	8
15 Feb 1990	NW	30	18
26 Sep 1987	NW	9	6
25 Aug 1987	S	23	14
18 Jul 1987	SE	32	26

Table 2. The 14 regional-scale flood events grouped into synoptic categories. The two first columns are the same as in Table 1. The third column refers to the synoptic categories, as defined in section 3. The forth column indicates the main direction of the IVT above the most affected regions during the heavy precipitation event.

Date	Affected region	Synoptic category	IVT direction
10 Oct 2011	NW	AR with NW flow	NNW
22 Dec 1991	NW	AR with NW flow	NW
15 Feb 1990	NW	AR with NW flow	WNW
12 May 1999	NE	AR with W-SW flow	WSW
26 Sep 1987	NW	AR with W-SW flow	WSW
08 Aug 2007	NE	PCO, early phase	NE
22 Aug 2005	NE	PCO	NNE
12 Aug 2002	NE	PCO	N
06 Aug 2000	NE	PCO	NNE
22 May 1999	NE	PCO	NNW
15 Oct 2000	SW	PV streamer	SSE
24 Sep 1993	SW	PV streamer	SSE
25 Aug 1987	S	PV streamer	S
18 Jul 1987	SE	PV streamer	SSW

Table 3. The 4 thresholds of IVT perpendicular to orography defined in this study. For each threshold, the right column indicates the number of exceedances related to each flood event (number of exceedances during the flood date and the day before). The number of other exceedances during the whole 33-year period (48212 time steps between 1979 and 2011) is also shown. Of the 14 flood events investigated, 4 did not exceed any of the 4 thresholds set. The maximum IVT intensity during these 4 cases is indicated at the bottom of the table.

350 $kg\,m^{-1}\,s^{-1}$ from NNW at 47°N-7°E	Exceedances
AR with NW flow on 10 Oct 2011	2
AR with NW flow on 22 Dec 1991	4
AR with NW flow on 15 Feb 1990	5
other exceedances between 1979 and 2011	3

300 $kg\,m^{-1}\,s^{-1}$ from NNW-ENE at 48°N-9°E	Exceedances
PCO on 22 Aug 2005	7
PCO on 12 Aug 2002	1
PCO on 06 Aug 2000	2
PCO on 22 May 1999	1
other exceedances between 1979 and 2011	7

400 $kg\,m^{-1}\,s^{-1}$ from 30° around SSE at 46°N-9°E	Exceedances
PV streamer on 15 Oct 2000	1
PV streamer on 24 Sep 1993	1
other exceedances between 1979 and 2011	0

550 $kg\,m^{-1}\,s^{-1}$ from 30° around S at 46°N-9°E	Exceedances
PV streamer on 25 Aug 1987	1
other exceedances between 1979 and 2011	1

Flood events without exceedances	IVT intensity
AR with W-SW flow on 12 May 1999	>P99
AR with W-SW flow on 26 September 1986	>P99
PCO on 08 Aug 2007	<P90
PV streamer on 25 Aug 1987	>P99

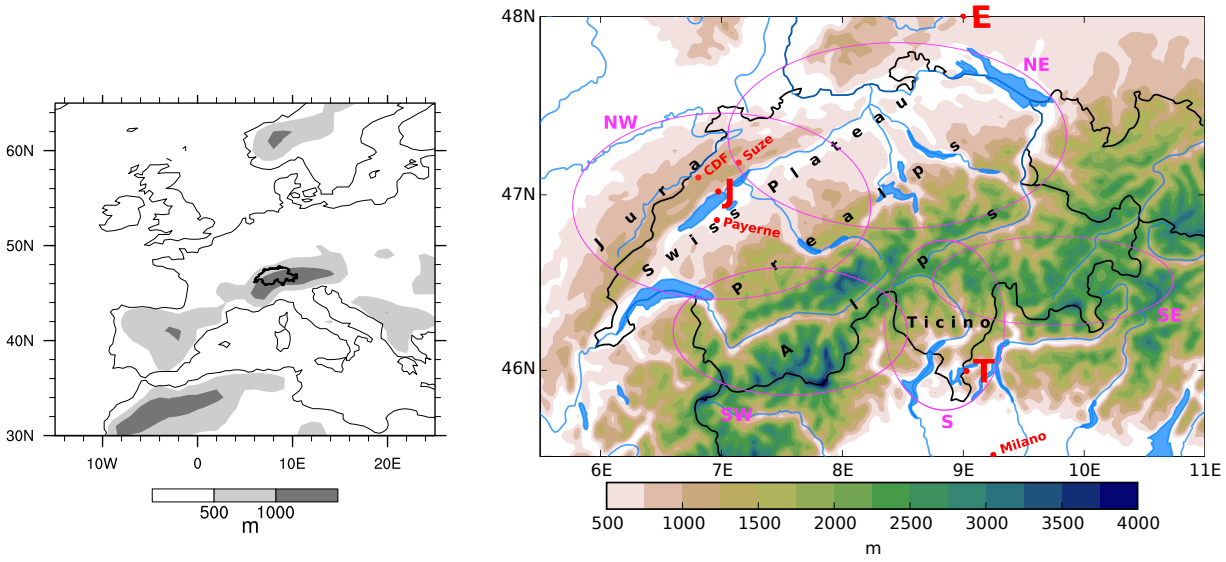

Figure 1. Left: Map of Europe with elevation in grey shadings. Switzerland is highlighted by a solid black line around its border. Right: Map of Switzerland with elevation in colour shadings; the network of Swiss rivers and lakes is shown in blue and the names of the main geographical regions are written in black. In this study, we refer to the zones delimited in pink as NW, NE, SW, S and SE Switzerland. Point locations referred to in the paper are marked in red: the Era-Interim grid points at 47°N-7°E, 46°N-9°E and 48°N-9°E are selected to represent the Jura Mountains (J), the Ticino (T) and eastern Switzerland (E) in this study; (CDF) indicates the location of precipitation and temperature station measurements at the city of La Chaux-de-Fonds; (Suze) indicates the location of a river discharge station along the Suze River; (Payerne) and (Milano) are two weather balloon launching stations from which data are assimilated in Era-Interim.

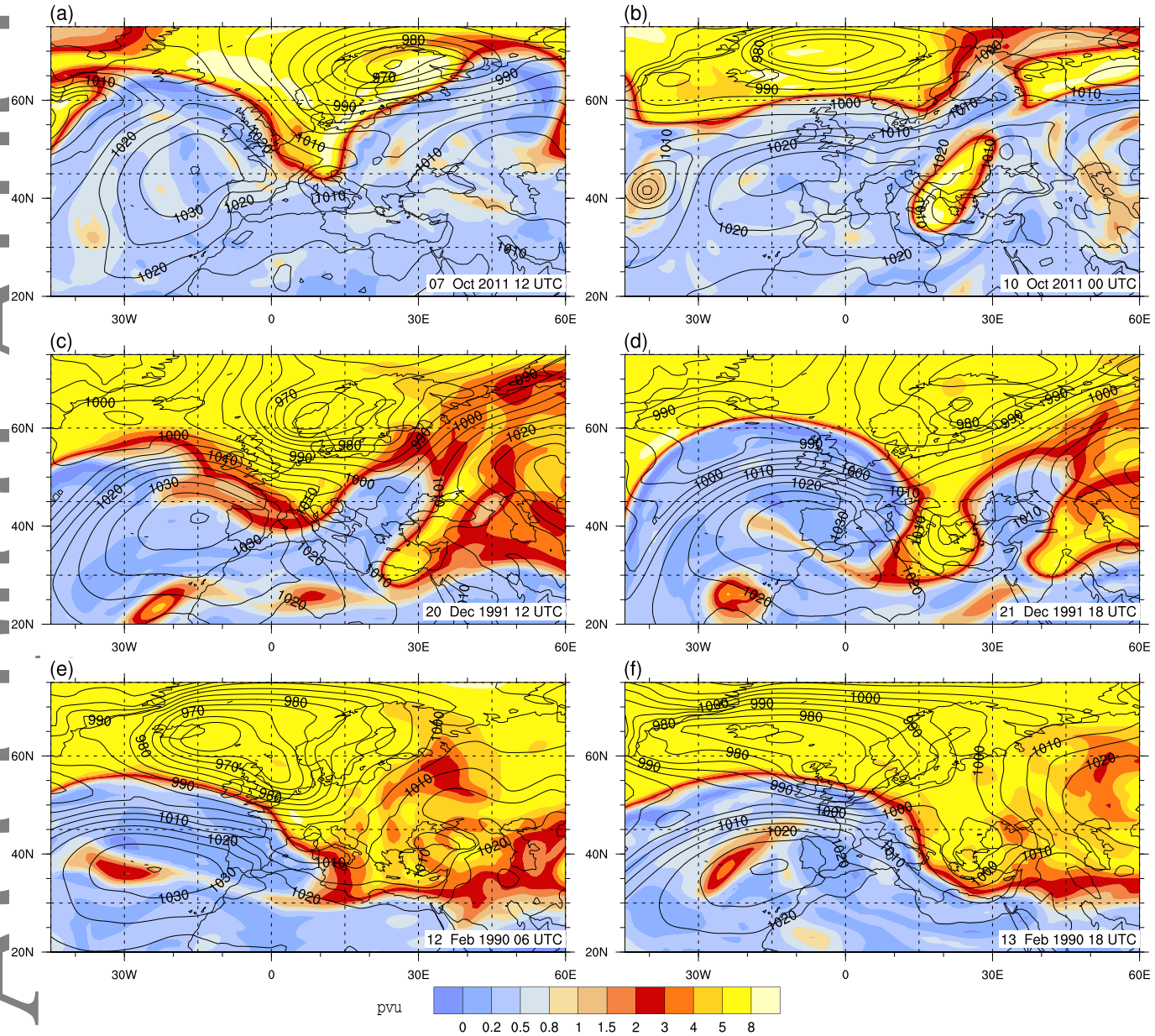

Figure 2. PV on the 320 K isentrope (colour shading, pv units pvu in 10^{-6} K m^2 kg^{-1} s^{-1}) and sea level pressure (black contours, hPa). The rows correspond from top to bottom to the flood events related to Atlantic ARs with NW flow in October 2011 (a-b), December 1991 (c-d) and February 1990 (e-f). The first phases of the events are shown in (a,c,e) and the second phases in (b,d,f).

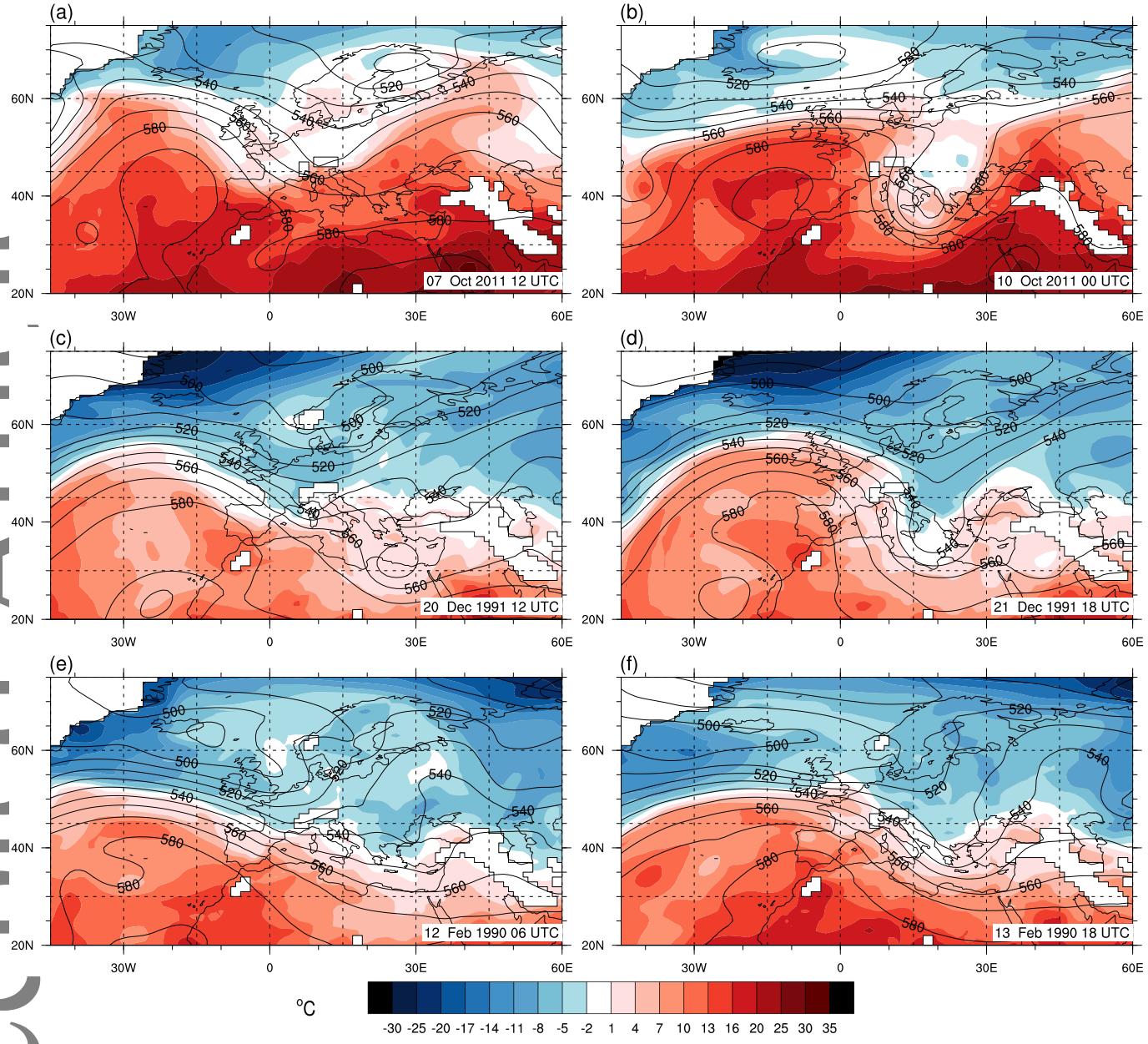

Figure 3. Temperature at 850 hPa (colour shading, °C) and geopotential height of the 500 hPa isobar (black contours, gpdm) for the same time steps as in Figure 2.

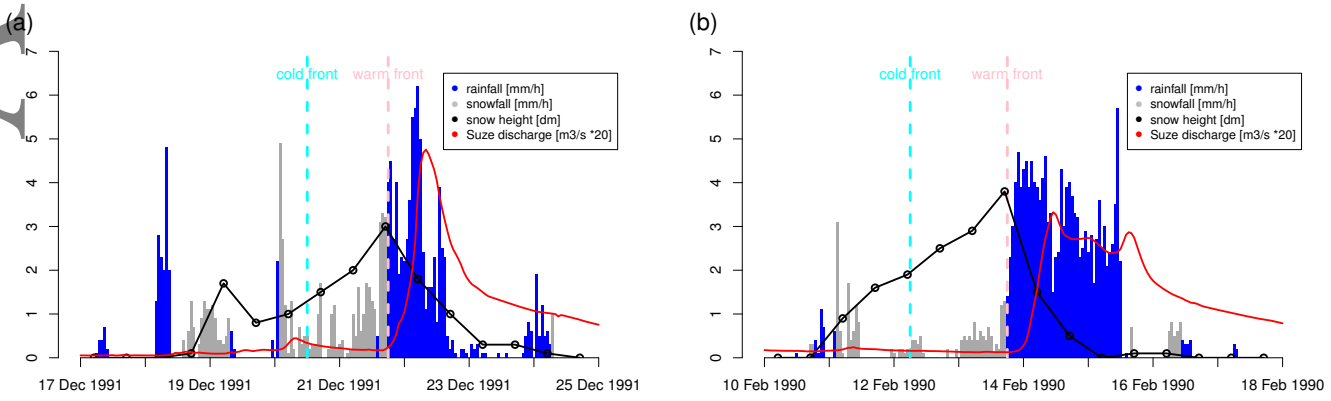

Figure 4. Surface conditions during two flood events affecting the Jura Mountains in December 1991 (a) and February 1990 (b). Time series of precipitation and snow depth were measured at La Chaux-de-Fonds, a city located at 1018 m a.s.l. in the Jura Mountains. River discharge was measured along the nearby Suze River (see the exact locations in Figure 1). Note that all variables are plotted against the same axis. Precipitation [mm/h] is separated into rainfall (blue bars) or snowfall (grey bars) based on the 2-meters temperature at La Chaux-de-Fonds (above or below 1.5°C). The measured total snow depth [dm] is shown with a black line. The hourly mean discharge of the Suze River [$m^3/s*20$] is shown in red. Vertical lines highlight the passage of fronts and correspond to the time steps in Figure 3(c,e) (cold fronts) and Figure 3(d,f) (warm fronts).

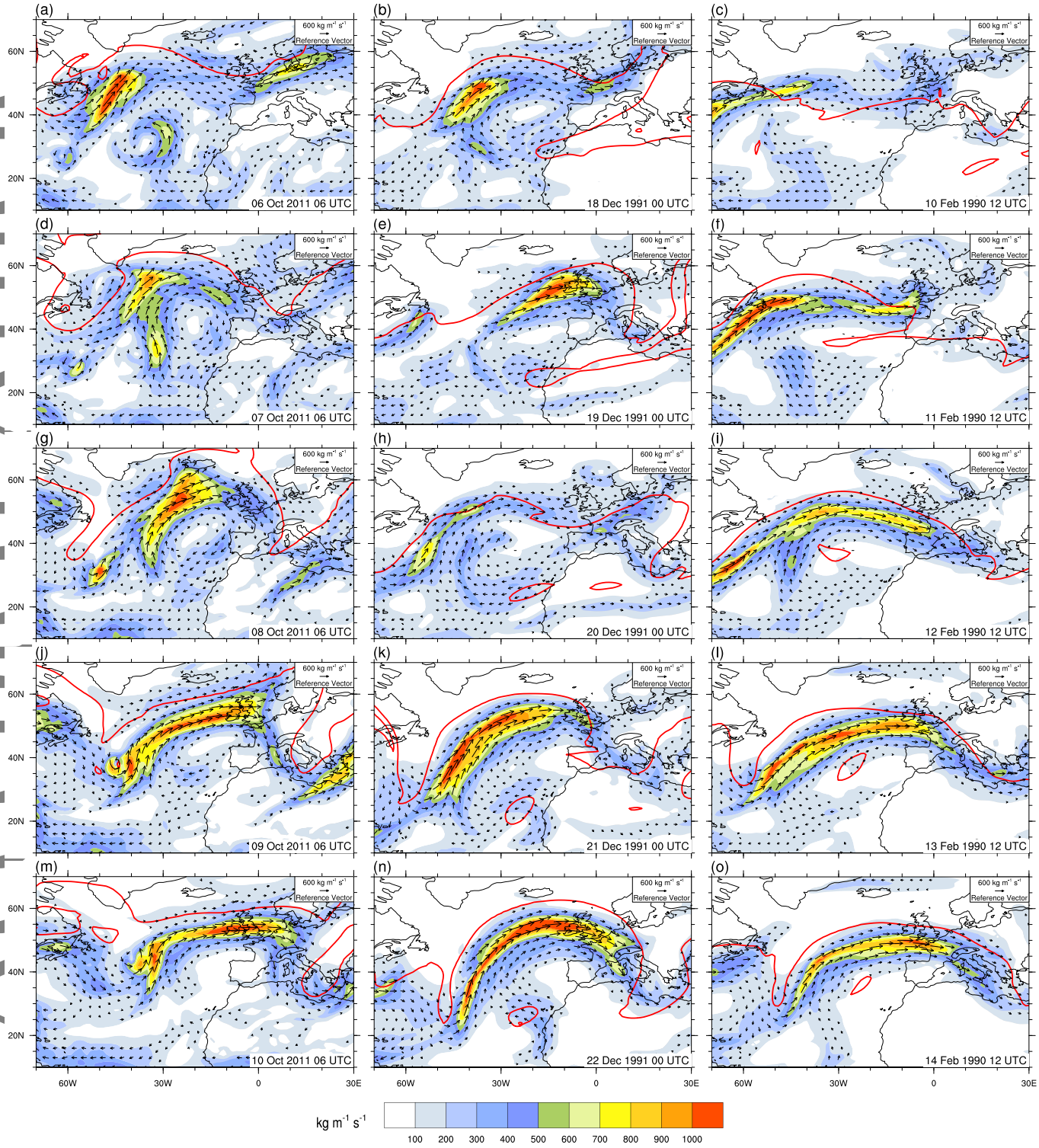

Figure 5. IVT amplitude (colour shading, $\mathrm{kg\,m^{-1}\,s^{-1}}$) and advection (arrows, $\mathrm{kg\,m^{-1}\,s^{-1}}$) and the dynamical tropopause (a red line shows the 2 PVU isoline on the 320 K isentrope). The three columns refer to the three flood events related to Atlantic ARs with NW flow. The panels from top to bottom show IVT over the Atlantic 4, 3, 2, 1 and 0 days before the ARs reached NW Switzerland. The IVT intensity peaked over NW Switzerland on 10 October 2011 06 UTC (m), on 22 December 1991 00 UTC (n) and on 14 February 1990 12 UTC (o). The Alps are highlighted by a black contour at 1000 m a.s.l..

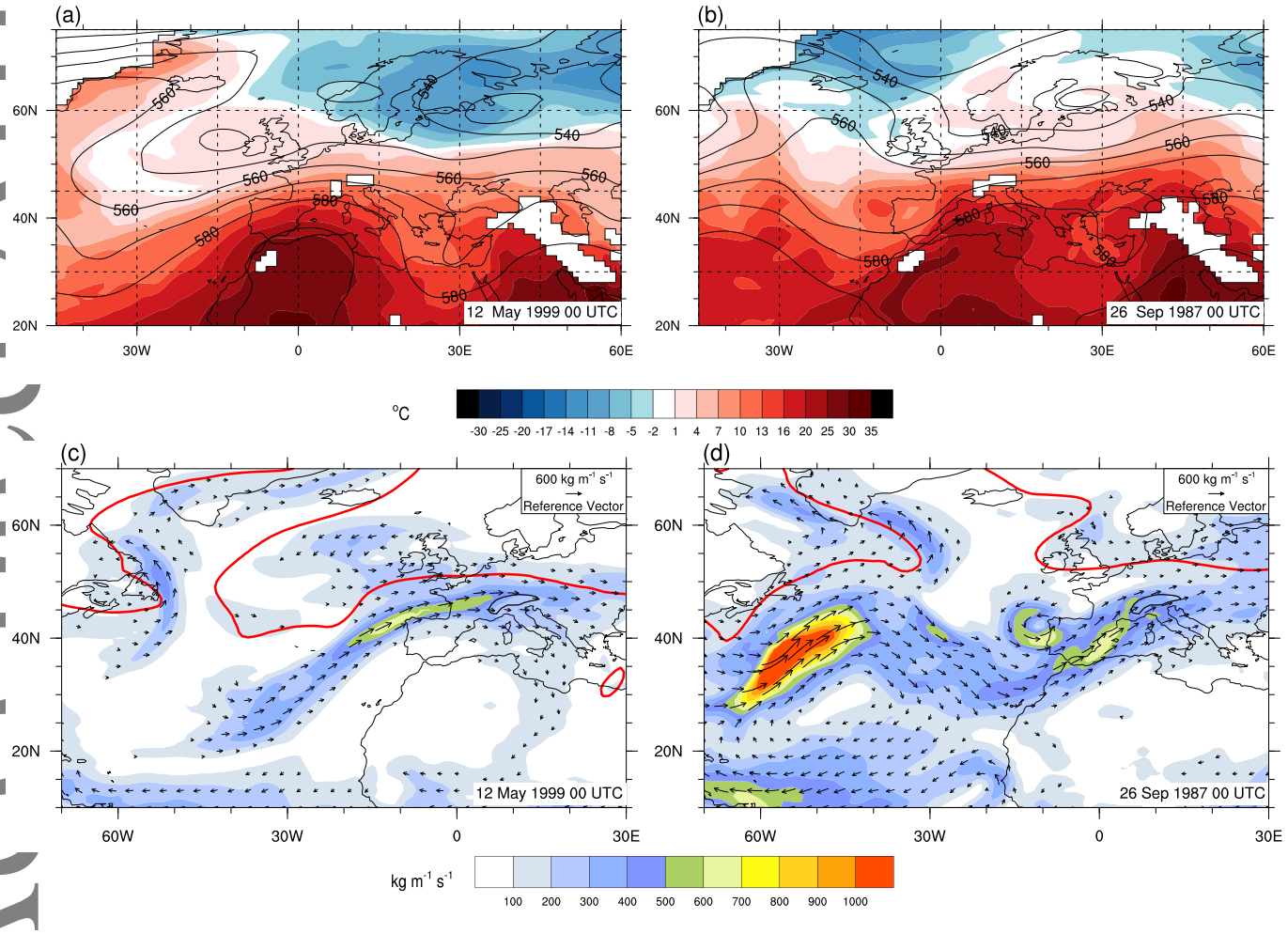

Figure 6. (a,b) Temperature at 850 hPa (colour shading, °C) and geopotential height of the 500 hPa isobar (black contours, gpdm). (c,d) IVT amplitude (colour shading, kg m^{-1} s^{-1}) and advection (arrows, kg m^{-1} s^{-1}) and the dynamical tropopause (a red line shows the 2 PVU isoline on the 320 K isentrope). The time steps correspond to IVT maxima over NE Switzerland during the two flood events related to ARs with W-SW flow in May 1999 (a,c) and September 1987 (b,d).

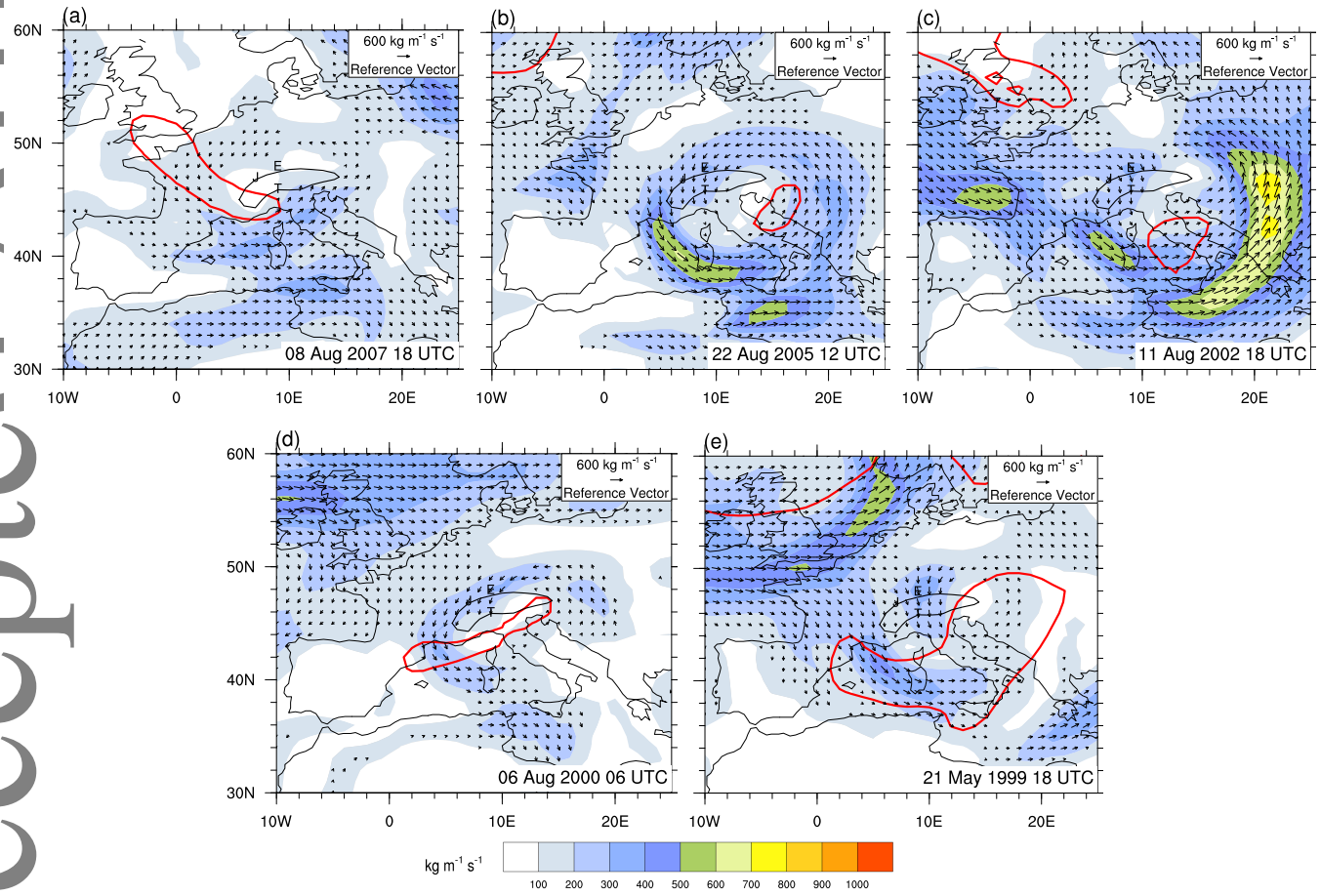

Figure 7. IVT amplitude (colour shading, $\mathrm{kg\,m^{-1}\,s^{-1}}$) and advection (arrows, $\mathrm{kg\,m^{-1}\,s^{-1}}$) and the dynamical tropopause (a red line shows the 2 PVU isoline on the 320 K isentrope). The time steps correspond to IVT maxima over NE Switzerland during the 5 flood events related to PCO-like situations. The Alps are highlighted by a black contour at 1000 m a.s.l. and the letters J, E and T refer to the locations in Figure 1.

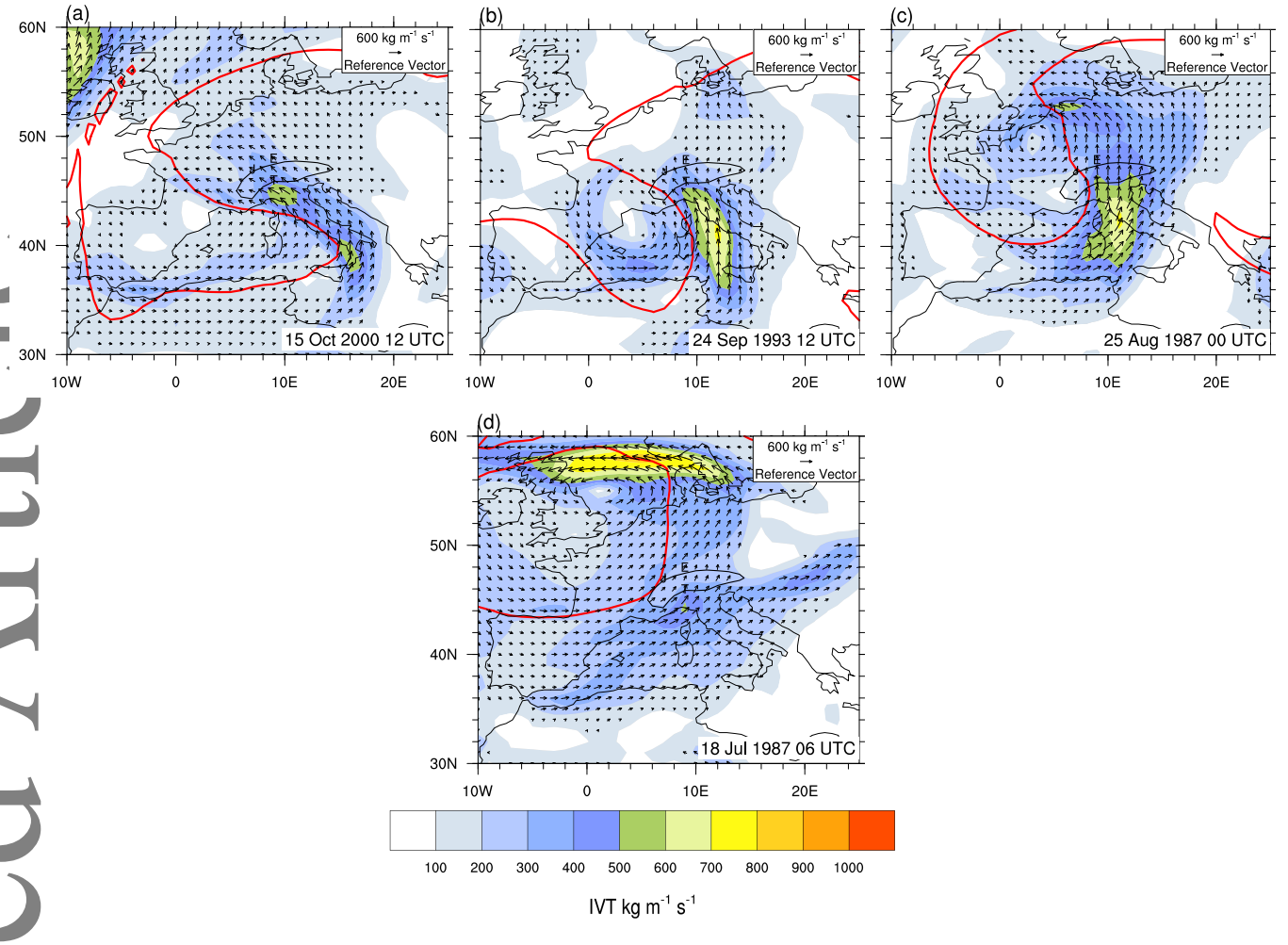

Figure 8. Same as Figure 7 but for time steps corresponding to IVT maxima over S Switzerland during the 4 events related to PV streamer-like situations. The red line shows the 2 PVU isoline on the 330 K isentrope.

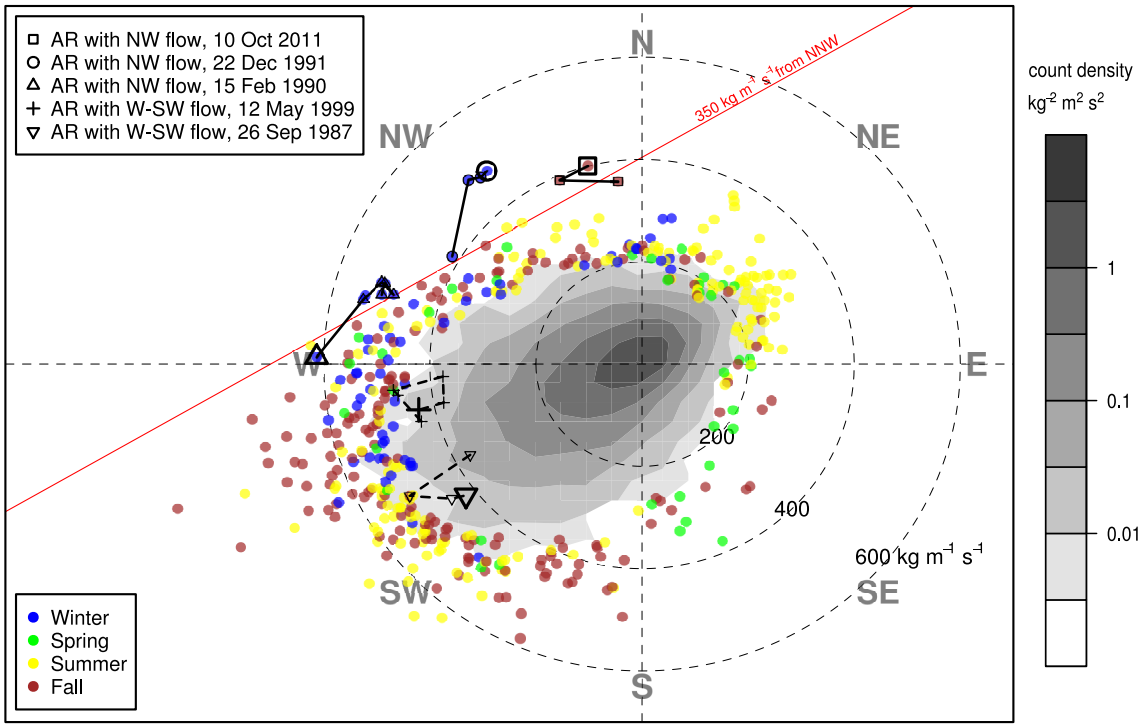

Figure 9. IVT climatology at the Era-Interim grid point 47°N-7°E (see Figure 1). The polar diagram contains IVT at every time step (every 6 hours over 33 years, resulting in 48212 values). The radial component indicates the intensity and the angle the direction of the IVT. Count density is shown with a logarithmic scale of grey shadings and the 1% most intense IVT values are represented with coloured dots (we calculated for each 5° direction bin the percentile 99 of the IVT intensity). Dot colours refer to the meteorological seasons. The highest IVT values from the flood dates and the preceding days are highlighted by symbols and connected by lines in chronological order (solid lines for ARs with NW flow and dashed lines for ARs with W-SW flow). The last highlighted time steps of the flood events (indicated by a larger symbol) are on 10 October 2011 06 UTC, 22 December 1991 12 UTC, 15 February 1990 12 UTC, 12 May 1999 18 UTC and 26 September 1987 12 UTC. A red line delimits an IVT component of 350 kg $m^{-1}s^{-1}$ from NNW.

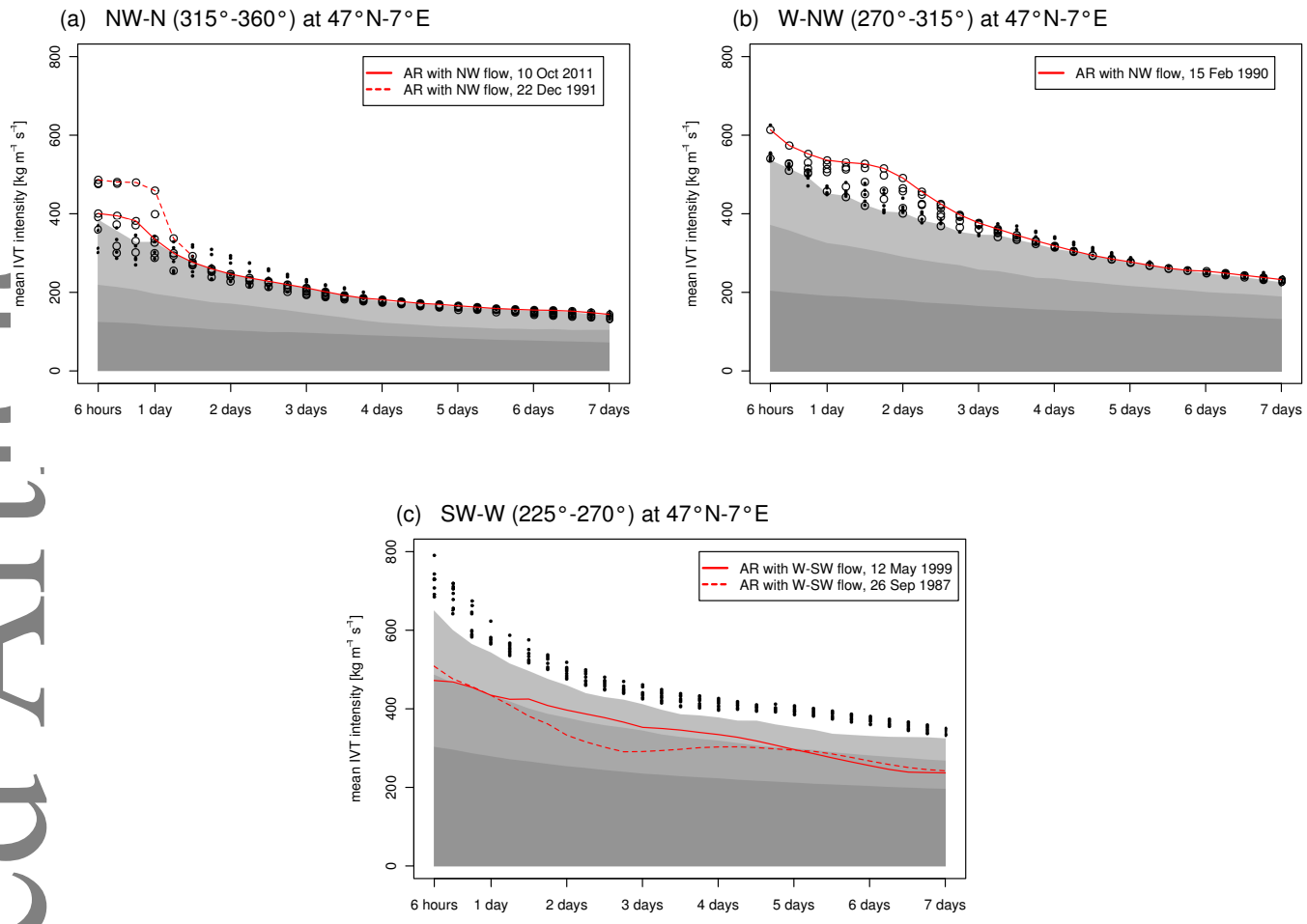

Figure 10. Intensity-duration-frequency (IDF) curves of IVT at 47°N-7°E and for IVT from the sector 315°-360° (a), 270°-315° (b), and 225°-270° (c). The dark grey, grey and light grey shadings cover areas below percentiles 90, 99 and 99.9 of each duration, respectively. The ten most intense IVT occurrences of each duration are indicated with open circles (dots) if they are (are not) related to one of the investigated floods. The red lines correspond to the events related to ARs with NW flow (a,b) and ARs with W-SW flow (c).

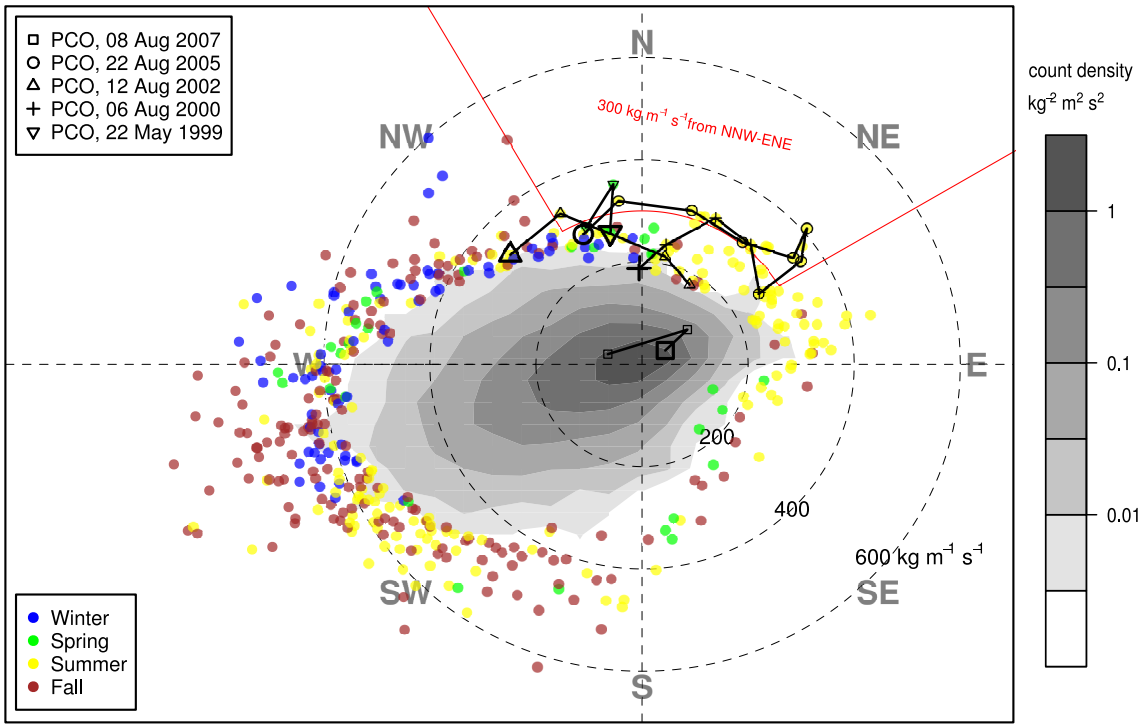

Figure 11. Same as Figure 9 but for the grid point 48°N-9°E and for the flood events related to PCO-like situations. The last highlighted time steps of the flood events are on 09 August 2007 00 UTC, 23 August 2005 00 UTC, 12 August 2002 00 UTC, 06 August 2000 18 UTC, and 22 May 1999 00 UTC. A red line delimits an IVT component of 300 kg m^{-1} s^{-1} from NNW-ENE.

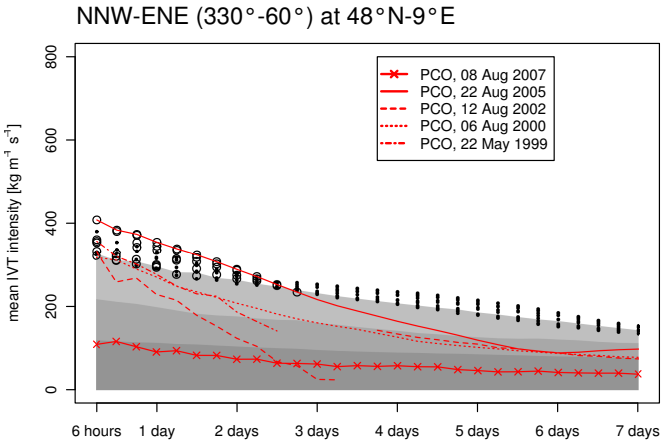

Figure 12. Same as Figure 10 but for the Era-Interim grid point 48°N-9°E and for the sector 330°-60°. The 5 flood events related to PCO-like situations are shown in red.

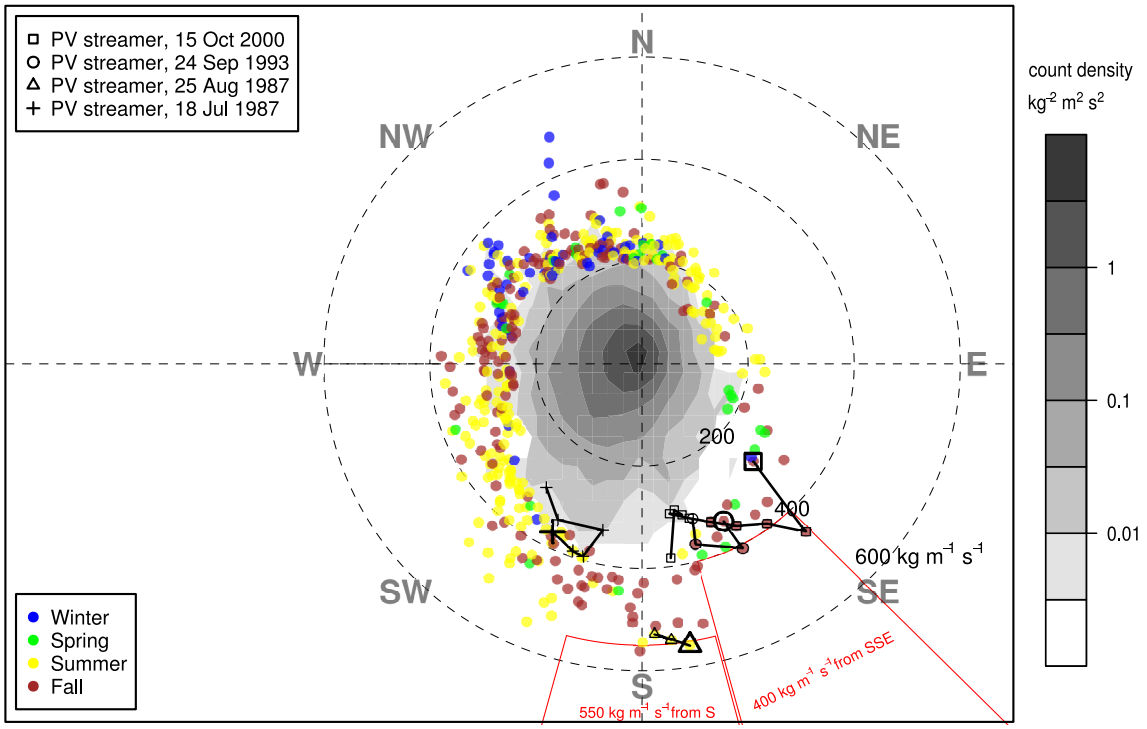

Figure 13. Same as Figure 9 but for the grid point 46°N-9°E and for the 4 flood events related to PV streamer-like situations. The last highlighted time steps of the flood events are on 15 October 2000 18 UTC, 24 September 1993 18 UTC, 25 August 1987 00 UTC and 18 July 1987 18 UTC. Red lines delimit IVT components of 400 kg m^{-1}s^{-1} from 30° around SSE (135°-165°) and 550 kg m^{-1}s^{-1} from 30° around S (165°-195°).

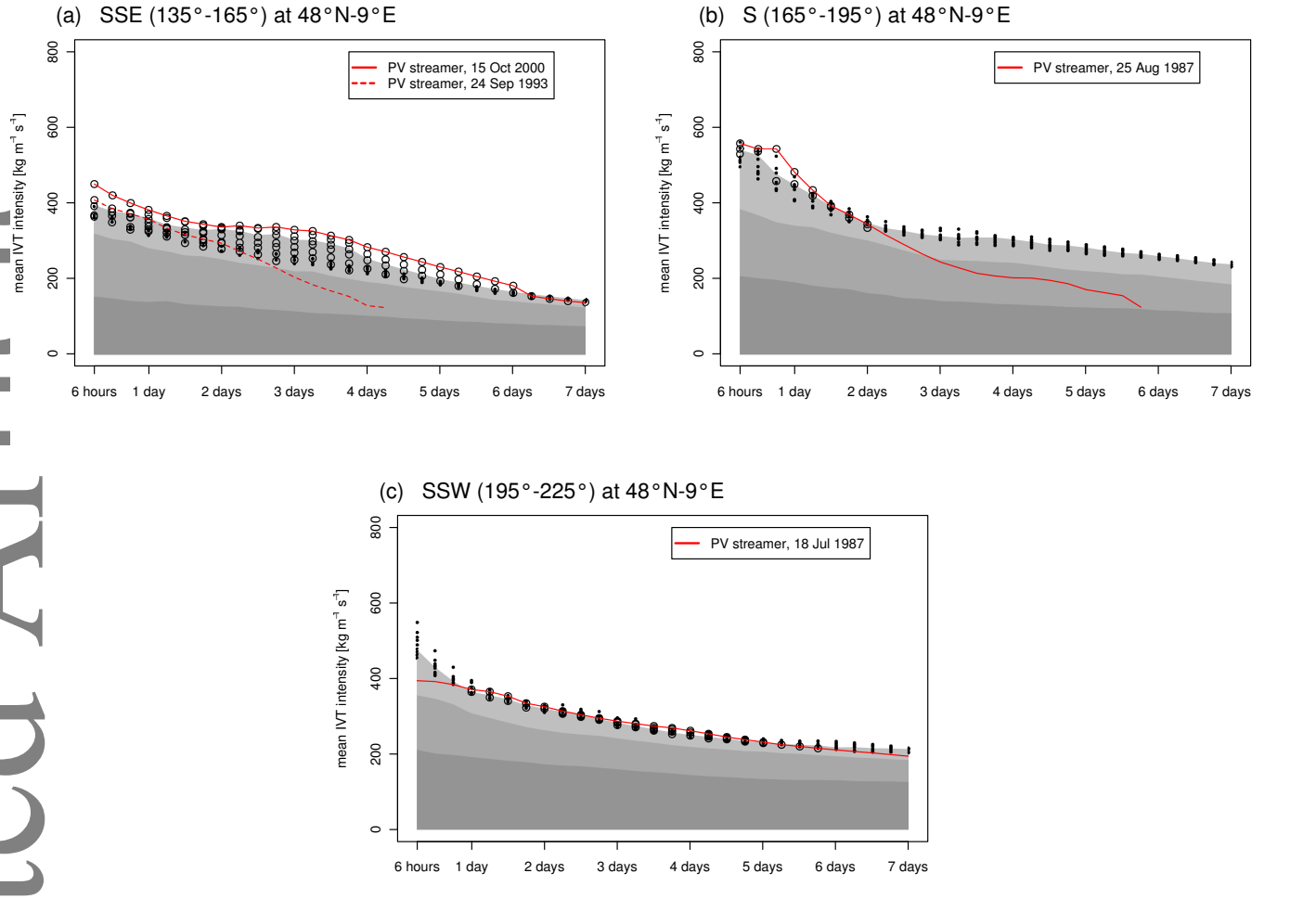

Figure 14. Same as Figure 10 but for the Era-Interim grid point 46°N-9°E and for the sector 135°-165° (a), 165°-195° (b), and 195°-225° (c). The 4 flood events related to PV streamer-like situations are shown in red.

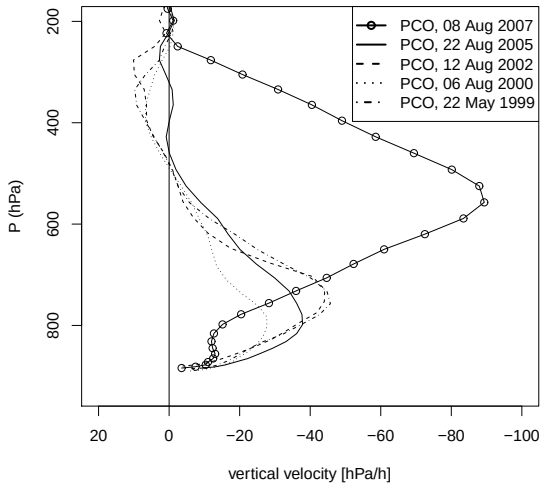

Figure 15. Vertical profiles of the vertical velocity [hPa/h] from Era-Interim at 47°N-8°E and for the 5 floods related to PCO-like situations. The times steps shown are 08 August 2007 18 UTC, 22 August 2005 12 UTC, 11 August 2002 18 UTC, 06 August 2000 06 UTC, and 21 May 1999 18 UTC.

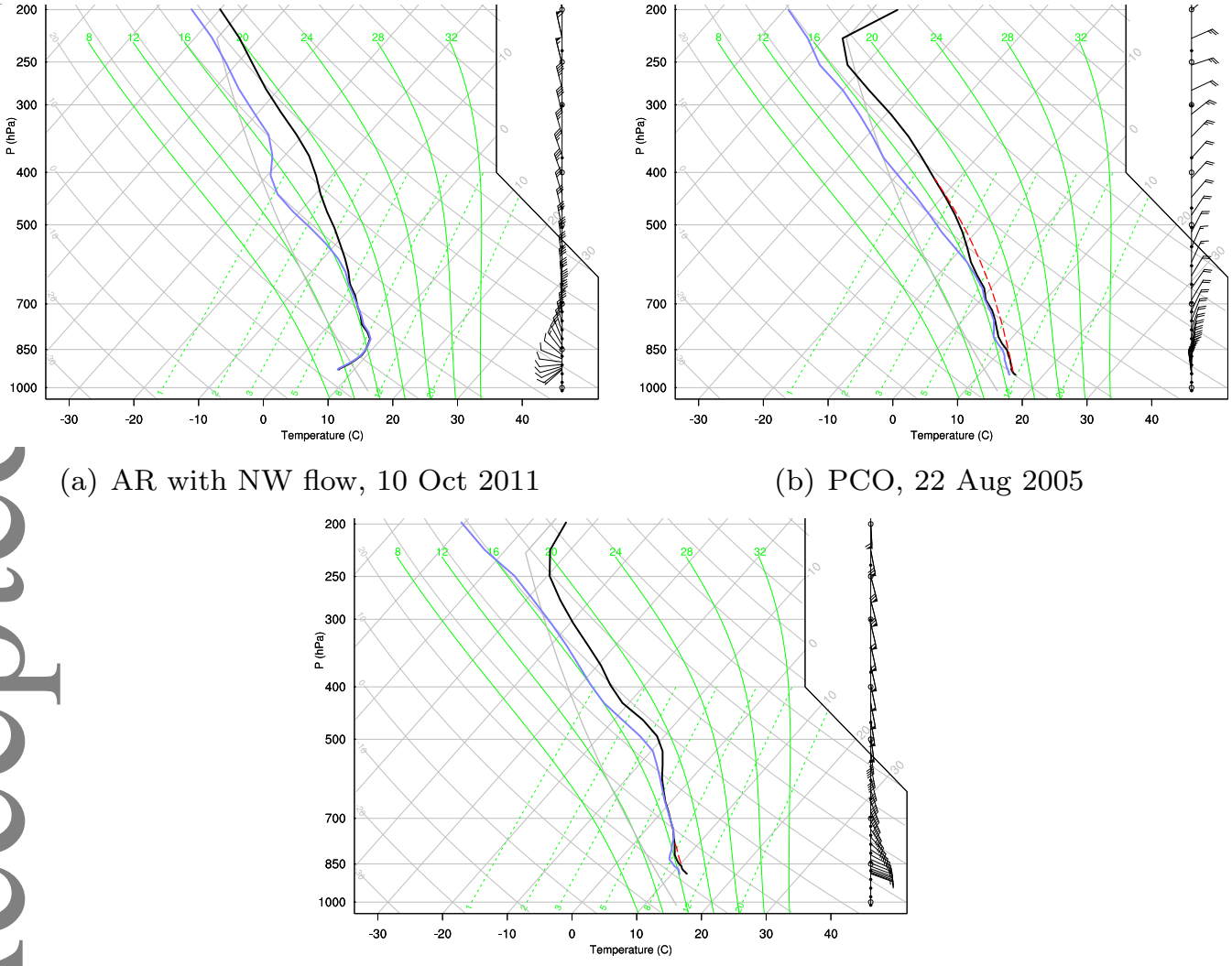

(a) AR with NW flow, 10 Oct 2011

(b) PCO, 22 Aug 2005

(c) PV streamer, 24 Sep 1993

Figure 16. Skew-T diagrams from Era-Interim profiles at 47°N-7°E on 10 October 2011 06 UTC (a), at 48°N-9°E on 22 August 2005 12 UTC (b) and at 46°N-9°E on 24 September 1993 12 UTC (c). Temperature is shown in black, dew point temperature in blue and the surface-based CAPE is proportional to the area between the red dashed line and the black line.